ISSN : 2165-4069(Online)
ISSN : 2165-4050(Print)

IJARAI

International Journal of
Advanced Research in Artificial Intelligence

Volume 5 Issue 8

www.ijarai.thesai.org

A Publication of
The Science and Information Organization

Editorial Preface

From the Desk of Managing Editor…

Artificial Intelligence is hardly a new idea. Human likenesses, with the ability to act as human, dates back to Geek mythology with Pygmalion's ivory statue or the bronze robot of Hephaestus. However, with innovations in the technological world, AI is undergoing a renaissance that is giving way to new channels of creativity.

The study and pursuit of creating artificial intelligence is more than designing a system that can beat grand masters at chess or win endless rounds of Jeopardy!. Instead, the journey of discovery has more real-life applications than could be expected. While it may seem like it is out of a science fiction novel, work in the field of AI can be used to perfect face recognition software or be used to design a fully functioning neural network.

At the International Journal of Advanced Research in Artificial Intelligence, we strive to disseminate proposals for new ways of looking at problems related to AI. This includes being able to provide demonstrations of effectiveness in this field. We also look for papers that have real-life applications complete with descriptions of scenarios, solutions, and in-depth evaluations of the techniques being utilized.

Our mission is to be one of the most respected publications in the field and engage in the ubiquitous spread of knowledge with effectiveness to a wide audience. It is why all of articles are open access and available view at any time.

IJARAI strives to include articles of both research and innovative applications of AI from all over the world. It is our goal to bring together researchers, professors, and students to share ideas, problems, and solution relating to artificial intelligence and application with its convergence strategies. We would like to express our gratitude to all authors, whose research results have been published in our journal, as well as our referees for their in-depth evaluations.

We hope that this journal will inspire and educate. For those who may be enticed to submit papers, thank you for sharing your wisdom.

Editor-in-Chief
IJARAI
Volume 5 Issue 8 August 2016
ISSN: 2165-4069(Online)
ISSN: 2165-4050(Print)

Editorial Board

Reviewer Board Members

CONTENTS

Improved Framework for Breast Cancer Detection using Hybrid Feature Extraction Technique and FFNN

Ibrahim Mohamed Jaber Alamin
Computer Science & Technology
University: Sam Higginbottom Institute of Agriculture Technology and Sciences Allahabad

Dr. W. Jeberson
Associate Professor, Dept. Of Computer Science & Technology, Sam Higginbotom Institute of Agriculture, Technology & Sciences -University, Allahabad

Dr. H K Bajaj
Md (Path), Dcp, Dept.: Health Sciences, Associate Professor, Sam Higginbottom Institute of Agriculture Technology and Sciences –University, Allahabad

***Abstract*—Breast Cancer early detection using terminologies of image processing is suffered from the less accuracy performance in different automated medical tools. To improve the accuracy, still there are many research studies going on different phases such as segmentation, feature extraction, detection, and classification. The proposed framework is consisting of four main steps such as image preprocessing, image segmentation, feature extraction and finally classification. This paper presenting the hybrid and automated image processing based framework for breast cancer detection. For image preprocessing, both Laplacian and average filtering approach is used for smoothing and noise reduction if any. These operations are performed on 256 x 256 sized gray scale image. Output of preprocessing phase is used at efficient segmentation phase. Algorithm is separately designed for preprocessing step with goal of improving the accuracy. Segmentation method contributed for segmentation is nothing but the improved version of region growing technique. Thus breast image segmentation is done by using proposed modified region growing technique. The modified region growing technique overcoming the limitations of orientation as well as intensity. The next step we proposed is feature extraction, for this framework we have proposed to use combination of different types of features such as texture features, gradient features, 2D-DWT features with higher order statistics (HOS). Such hybrid feature set helps to improve the detection accuracy. For last phase, we proposed to use efficient feed forward neural network (FFNN). The comparative study between existing 2D-DWT feature extraction and proposed HOS-2D-DWT based feature extraction methods is proposed.**

Keywords—Breast Cancer; Preprocessing; Segmentation; Region Growing; Noise Removal; Filtering; Orientation; Gradient Magnitude; Higher Order Statistics; FFNN

I. INTRODUCTION

Cancer is the major threat for human being health and its number of patients increasing word wide due to the global warming, even if there are new therapies and treatments proposed by research doctors, but level of cancer defines the ability of its cure. There are different types of cancers from which human being is suffering [male and female]. In this paper we are focusing on breast cancer in women, rest all cancers are out of scope of this paper. Large number of women population is affected by the breast cancer. A different type of reasons causes the breast cancer such as X-Ray [1]. For women's, breast cancer is most common cancer, and it has been increasing since from last decade. The countries like under developed and developed in which breast cancer is commonly observed in females. The estimation of death caused by breast cancer for every year is approximately 40,000 females. This estimation is measured by WHO (world health organization). The world health organization is recognized organization for conducting the research on different cancer diseases. The world health organization also provides the number of breast cancer diagnosis approximately around 200,000. The breast masses evaluation in men is same as in women by considering the mammography [2]. The objective of mammography is conduct the early detection test for breast cancer disease. Mammography is performed based on masses properties as well as micro calcifications. Mammography technology helps to detect the breast cancer before it can happen to individual. But still this approach is not completely accurate. In addition to this, for radiologists it is difficult task to find out the difference between the malignant tumors as well as benign tumors. In mammography, presence of breast cancer is basically reflected. The present approaches considering that recording of image is done over the X-ray film and then that image is interpreted by the medical expertise. However, such approaches are highly vulnerable to visual inspection error and human error. This can be later improved by mammogram images which is of poor quality. The early detection rate is increases based on automated analysis mammogram screening as per the reviews and instigations by different researchers. Another approach is screening mammography which is accurate radiological method currently available for early detection of breast cancer. However as the large number of mammograms needs the analysis, false detections resulted from the radiologists. Therefore, novel techniques for automatic and scalable detection are applicable to overcome such problems. The detection or segmentation of micro-calcification supporting the digital mammogram screening in order divide the clusters as benign or malign [2].

The reason for detection of early breast cancer is that it can helps to cure breast cancer via the proper treatment completely. Such early detection are done by the self-examination process in every month for woman in earlier days. But as discussed in

above paragraph, since from last decade mammography approach is used by many doctors and hospitals for early detection of breast cancer. Micro calcifications and masses characteristics are helps to detect the early cancer for particular individual and hence these are vital factor in detection process. X-ray machines are used to perform the mammography test over the naked upper part of individual. Here in detail mammography is performed as both breasts of women are compressed between the 2 plates with goal of capturing the both photos every breast with help of X-ray pulse. Other well-known methods for early detection breast cancer are CAD (computer aided detection), clinical breast analysis, and blood tests. In order to cure breast cancer completely, it becomes very important to detect it early [3] [4].

CAD becomes interesting area of research since from last decade for early detection of breast cancer to number of researchers as there are number of CAD based automated methods presented by various researchers. The objective of CAD technique is to support radiologists in analysis of breast images by giving the second opinion. The vital goal of CAD is to detect the breast cancer early in women's. Methodology of CAD is based on more than one technique consisting of image preprocessing methods to recognition methods CAD for the detection of CAD based abnormalities in mammograms of breast cancer image. Since from last two decades, number of research groups presented their studies on computer aided diagnosis for early breast cancer detection based on image processing terminologies. CAD takes input as computerized mammographic image which can be generated from the digitally acquired mammogram or traditional film mammogram [4].

The system which is designed based on computer helps to find the abnormal regions of mass, density and calcification in order to diagnose the presence of breast cancer in input image. After detection of this regions, CAD tool highlighting such regions over the original image with aim of further analysis by radiologist. CAD methodology supporting radiologists to make patient management by providing the different recommendations. Since from last 5-7 years, there many advanced CAD systems are proposed by researchers with goal of improving efficiency and accuracy of early breast cancer detection and the objective of assisting the radiologists in interpretation of medical images by providing a second opinion [6] [7]. An important application of CAD is in the diagnosis of breast cancer, which is a common form of cancer diagnosed in women. CAD is an interdisciplinary field, involving elements from basic image processing to advanced machine learning techniques. Therefore use of CAD based detection techniques use is increasing in which image processing concepts are used on input photos from X-ray for automatic detection of breast cancer with its level. CAD system helping to save efforts, time and costs factors for hospitals and doctors. Image processing is nothing but physical method and it is applied in order to convert the breast image signal into the physical image. The image signal is also known as digital image signal, and output of this process is either physical image or its related characteristics. Breast cancer detection is wide range of research in which different researchers preparing their research articles and proposing the new techniques and solutions for breast cancer detection with practical evaluation using the image processing concepts. CAD based techniques are composed of several steps to detect the early detection of breast cancers like acquisition of image, preprocessing of image, segmentation of image, possible feature extraction and then classification for diagnosis. This research paper is contributed by presenting three different phases and algorithms for improving the overall accuracy of breast cancer detection. In this paper contribution is done in four main phases in this work such as preprocessing, image segmentation, feature extraction and classification. Our contributions showing that proposed work improved the detection accuracy as compared to existing approach. In rest of this paper, section II is discussing about the different methods of presented so far on automated breast cancer detection framework. Section III is showing the proposed algorithm, its steps, and inside details for breast image segmentation. Section IV is showing the practical results for this segmentation work on different breast cancer images. Section V presents the conclusion and future work.

II. Related Works

The literature review study of existing methods is considered as one of the important factor that keep the foundation of further system enhancement and development. Therefore, in order to get the information about the existing approaches or systems for breast cancer detection CAD system, a review has been prepared. Below recent ten methods are listed and discussed below for breast cancer detection based on terminologies of CAD system.

- In [4], author Pawar, P.S. et al proposed the novel CAD system architecture for breast cancer detection by implementing back propagation neural network and the authors compared their work with radial basis function network for performance evaluation. The results obtained justifies that back propagation based system performs better for detect breast cancer.
- In [5], author Sameti, M. et al introduced the new image feature extraction technique for the analyzing the screening mammograms retrospectively. This method is taken prior to the detection of a malignant mass in order to detect early breast cancer. For individual mammographic projections of the malignant breast the two specific regions were categorized. The first was for malignant mass subsequently developed and another for similar to region one on the same mammogram. The author employed a stepwise discriminant analysis that exhibited that most of the features could be employed for highly effective classification process of malignant and benign cancer.
- In [6], author Sajjadieh, M.H.S. et al introduced the clutter suppression method referred as DAF/EDF technique which is helps in isolating tumor response from the complete response of tumor and clutter successfully. The presented approach by author is mainly consisting of DFA (data adaptive filter) as well as EDF (envelope detection filter) methods. The benefits of DFA and EDF is that they does not needs any prior training. The implementation approach

followed by authors in which DAF and EDF methods are coupled with TR (time reversal) array method of imaging. This system was analyzed by executing finite difference and time difference (FDTD) electromagnetic simulations depending on MRI (magnetic resonance imaging) of breast data. For microwave detection, this approach was efficient.

- In [7], authors Padmanabhan, S. et al presented the another approach with goal of improving the diagnostic accuracy of early breast cancer using digital mammograms by adopting the simulation tools such as MATLAB with dataset of MIAS. During this work, author introduced the approach for tumor cells detection in order to segment them in various disease phases. Authors also considering the approach of object detection, its recognition and mammograms classification with goal of presenting the difference among abnormal and normal cells. In their study, it was noticed that dense breasts can resulted into more difficult for interpretation with conventional mammograms.
- In [8], author Ben Hamad, N et al presents the study over optimum wavelet approaches and its optimal potential level of decomposition that could provide higher detection accuracy. In the two stage system the author performed multi resolution analysis on the basis of 1D discrete wavelet transform over profiles of micro-calcifications extracted from mammographic images. This was grow up by results validation with the consideration of 2D DWT (discrete wavelet transform) in phases of analysis as well as synthesis over the screening mammograms those are extracted from the MIAS dataset for the micro-calcifications detection.
- In [9], Sridhar, B. et al introduced the approach for automatic image segmentation with goal of tumor detection. The CAD system was designed by authors for the detection of malignant and benign from the images of CT (computed tomography). In their work they employed curvelet transform technique for image segmentation and feature extraction. The main goal of this work was to explore the robustness of curvelet transform which is a multi-scale transform that can represent the edges along curves much more efficiently.
- In [10], author Hussain, M. et al introduced the approach for kernel functions implementation for the early breast cancer diagnosis. The author focused on SVM implementation for the task of classification by considering the various functions of kernel.
- In [11], author Yao-lin Li et al presented function of mixture membership based on the linear distance membership as well as tight density membership. Author focused on efficient classifier design for improving the detection accuracy.

III. METHODOLOGY

The proposed methodology is described in below three contribution points in order to overcome the research challenges of existing automated methods of breast cancer detection in early stage.

- Preprocessing efficiency, in this work we have designed new combined approach for getting better. This preprocessing step is combination of filters like Laplace filter, smooth filter and then binarization and finally smoothing operations. This improves the quality of input raw image more as compared to previous basic preprocessing steps.
- Next contribution of this thesis is used of efficient segmentation method. The existing approach of region growing method is having constraints of orientation and intensity while image segmentation. Therefore the new modified region growing technique is proposed to overcome such constraints by considering both orientation and intensity for efficient image segmentation.
- Feature extraction methods, this is another area in which it is required to have efficient technique in order to get improved recognition accuracy. We proposed the hybrid feature extraction technique which is combination of texture, gradient magnitude, DWT+HOS etc. Another sub contribution is the use of efficient FFNN classifier as compared to existing classifiers.

As per method and flow defined in figure 1 below, three main algorithms are discussed below for preprocessing, segmentation and feature extraction. After that FFNN classifier is applied to get classification accuracy.

Algorithm 1: Preprocessing Algorithm

Step 1: Breast Image Browsing

Step 2: The input raw image needs to be preprocessed.

Step 3: The input image is first resized into 256 * 256 size using the MATLAB function of image resize.

Step 4: 2D conversion, if the input image is 3 dimensional (3D) then it is first converted into 2D, as most of image processing methods are applied on 2D images only. In short, RGB image is converted into gray scale image.

Step 5: Image de-noising is applied by using two filtering techniques mentioned in below steps: Step 5.1: Out_1 = apply Laplacian filter on grayscale image

Step 5.2: Out_2 = apply mean filter on grayscale image

Step 5.3: Out_3 = Out_1 – Out_3

Step 5.4: Out_3 is final preprocessed image

Step 6: Preprocessed breast image

Algorithm 2: Improved Region Growing Segmentation

Input: Out_3 image [Preprocessed Image]

Step 1: Out_3 is preprocessed image from gradient is extracted over X and Y axis in variables OutX and OutY.

Step 2: Combining gradient values using the below equation to get gradient vector Gval.

Gval =[1/(1+(OutX+OutY))]

Step 3: Gval is in radians; hence it is converted to values of degrees in order get orientation information of image pixels.

Step 4: Image Out_3 is divided into grids GRi.

Step 5: Define the threshold values for intensity and orientation in variables Ti and to respectively.

Step 6: for each GRi do

6.1. Compute the histogram Hi of each pixel Pj over grid GRi.

6.2. Searching the frequent histogram of Find the most frequent histogram of GRi grid and referred as FreqH.

6.3. Choose any pixel Pj related to FreqH value, and then assign that pixel information seed point (SP) which is having Ip [Intensity value] and Op [Orientation value].

6.4. Checking the constraint such as intensity and orientation constraints for neighbouring pixel.

6.5. If both a constraint satisfied, then region is grown, else next GRi grid is taken for further processing.

Step 7: Segmented Image

Algorithm 3: Feature extraction algorithm

Input: Segmented Breast Image

Step 1: Extract Texture Features from Input and form feature vector GeF

Step 2: Extract Gradient Features: Gradient and Direction

Step 2.1: Apply mean and standard deviation on gradient

Step 2.2: Apply mean and standard deviation on direction

Step 2.3: Form final 4 features gradient vector called GrF

Step 3: Apply 2D DWT

Step 3.1: Apply mean and standard deviation on LLD

Step 3.2: Apply mean and standard deviation on LHD

Step 3.3: Apply mean and standard deviation on HLD

Step 3.4: Apply mean and standard deviation on HHD

Step 3.5: Form final 8 feature 2D-DWT feature vector called DiF.

Step 4: Apply and Extract Higher order statics using skewness and kurtosis and store all features in vector HoF.

Step 5: Combine GeF, GrF, DiF and HoF to form hybrid feature vectors called CHF.

Output: Feature Vector CHF.

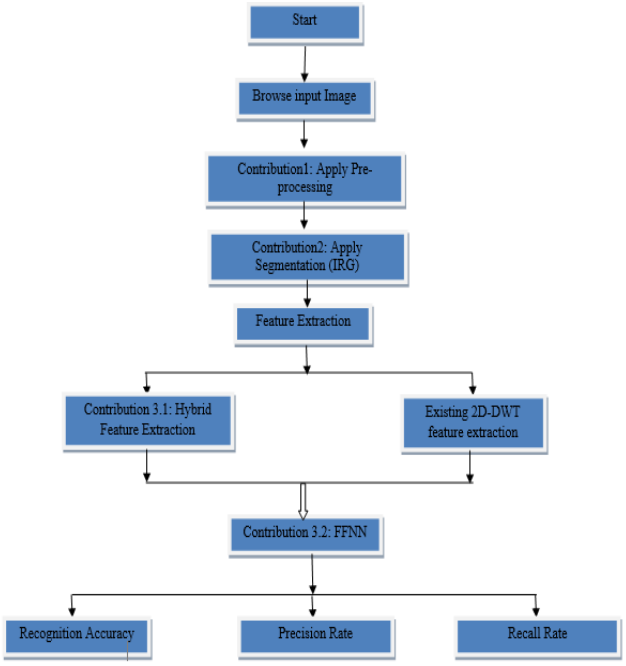

Fig. 1. System Architecture and Flowchart

IV. Experimental Results

A. ***Dataset Information:*** Number of research datasets for breast images is publically available for research studies. For this research two well know datasets such as Mammographic image analysis society (MIAS) and digital database for screening mammography (DDSM) are used. These two datasets are widely used for CAD systems and research works. This dataset we divided into two main classes normal and abnormal with varying number of image samples such as 30, 60, 90, 120, 150 and 180 per class for training and classification purpose.

B. ***Performance Results***

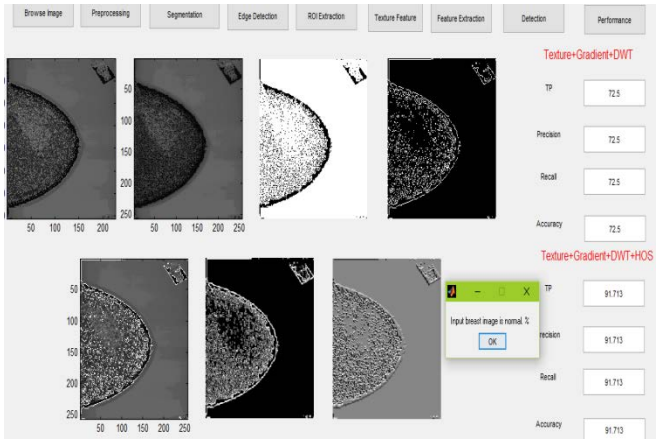

Fig. 2. GUI for proposed framework of automatic detection of breast cancer based on input breast image

Above figure 2 is showing the outputs of all steps and algorithm proposed in this paper such as first task is preprocessing whose output is showing in second window, next is image segmentation using proposed modified region growing technique and its output is showing in window 3 in above figure. After that edge detection, ROI extraction and proposed method of hybrid feature extraction is done. Based on extracted features, classification is done to detect the class of input image whether it is normal or having cancer. Below tables showing the performance analysis for correct classification accuracy and incorrect classification accuracy in between existing and proposed method for varying number of training size. Table 1 showing the comparative study between existing method and proposed method for overall classification accuracy according to varying training sample size.

TABLE I. CLASSIFICATION ACCURACY PERFORMANCE ANALYSIS

Training Size	Existing Method Accuracy (%)	Proposed Method Accuracy (%)
30	72.5	91.71
60	73.1	79.17
90	75.003	81.7
120	70.27	75.71
150	77.57	80.8
180	66.78	81.5

TABLE II. INCORRECT CLASSIFICATION PERFORMANCE ANALYSIS

Training Size	Existing Method Accuracy (%)	Proposed Method Accuracy (%)
30	27.5	8.28
60	26.89	20.82
90	24.99	18.29
120	29.72	24.28
150	22.42	19.19
180	33.21	18.49

From above table 1 and 2, it is clear that proposed method for automatic breast cancer detection is performing better as compared to existing method for all types of training sizes. The performance analysis for correction classification and incorrect classification is depicted in table 1 and 2 respectively. Figure 3 is showing the comparative graph analysis for detection accuracy of 2D-DWT based system and proposed 2D-DWT + HOS feature extraction methods.

V. CONCLUSION AND FUTURE WORK

The goal of this research article is to focus on improving the detection accuracy of CAD technique for breast cancer detection. By considering this objective, this paper presenting the contribution, its framework, flowchart and parameters with simulation environment. Based on this proposed work methods, simulation study is conducted by using publically available research dataset for normal and abnormal breast images of different candidates. The experimental results introduce the goal and main contribution of this research work. The automated computerized breast cancer detection framework presented in this thesis is having maximum accuracy is around 91 % under real time simulation environment which is more as compared to existing or previous methods which are based on SVM-model and 2D-DWT or relevant features extraction techniques. The maximum accuracy of existing methods is around 77 % for correct classification. Therefore, proposed approach of breast cancer detection improving the overall accuracy by 15 % in an average for all sizes of training. The possible future work for this to extend this work by online breast cancer detection system as current system is offline.

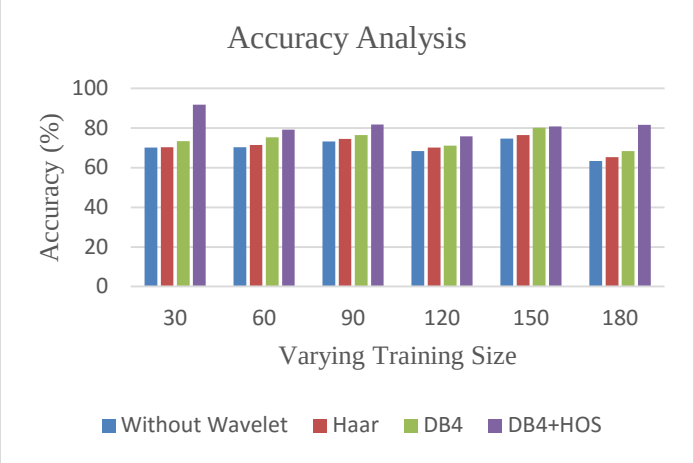

Fig. 3. Comparative analysis of different CAD methods

REFERENCES

[1] Babu, G.A.; Bhukya, S.N.; Kumar, R.S., "Feed forward network with back propagation algorithm for detection of breast cancer," Computer Science & Education (ICCSE), 2013 8th International Conference on 26-28 April 2013, vol., no., pp.181-185.

[2] Oral, C.; Sezgin, H., "Classification of mammograms using multilayer neural network," Electrical, Electronics and Computer Engineering (ELECO), 2010 National Conference on 2-5 Dec. 2010, pp.512-515.

[3] Alias, Norma; Ghani, A.C.A.; Saipan, H.F.; Ramli, N.; Palil, S.Q.M., "Wave equation for early detection of breast cancer growth using MATLAB Distributed Computing," Enabling Science and Nanotechnology (ESciNano), 2012 International Conference on 5-7 Jan. 2012.

[4] Pawar, P.S.; Patil, D.R., "Breast Cancer Detection Using Neural Network Models," Communication Systems and Network Technologies (CSNT), 2013 International Conference on , vol., no., pp.568,572, 6-8 April 2013.

[5] Sameti, M.; Ward, R.K.; Morgan-Parkes, J.; Palcic, B., "Image Feature Extraction in the Last Screening Mammograms Prior to Detection of Breast Cancer," Selected Topics in Signal Processing, IEEE Journal of , vol.3, no.1, pp.46,52, Feb. 2009

[6] Sajjadieh, M.H.S.; Asif, A., "Unsupervised time reversal based microwave imaging for breast cancer detection," Electrical and Computer Engineering (CCECE), 2011 24th Canadian Conference on 8-11 May 2011, vol., no., pp. 1411- 1415.

[7] Padmanabhan, S.; Sundararajan, R., "Enhanced accuracy of breast cancer detection in digital mammograms using wavelet analysis," Machine Vision and Image Processing (MVIP), 2012 International Conference on 14-15 Dec. 2012 vol., no., pp.153-156.

[8] Ben Hamad, N.; Ellouze, M.; Bouhlel, M.S., "Wavelets investigation for computer aided detection of microcalcification in breast cancer," Multimedia Computing and Systems, 2009. ICMCS '09. International Conference on 2-4 April 2009, vol., no., pp.547-552.

[9] Sridhar, B.; Reddy, K.V.V.S., "Qualitative detection of breast cancer by morphological curvelet transform," Computer Science & Education (ICCSE), 2013 8th International Conference on , vol., no., pp.514,517, 26-28 April 2013.

[10] Hussain, M.; Wajid, S.K.; Elzaart, A.; Berbar, M., "A Comparison of SVM Kernel Functions for Breast Cancer Detection," Computer Graphics, Imaging and Visualization (CGIV), Eighth International Conference on 17-19 Aug. 2011, vol., no., pp.145-150.

[11] Yao-lin Li; Jun Feng,; Yan Ren; Qiu-ping Wang; Bao-ying Chen, "Breast cancer detection based on mixture membership function with MFSVM-FKNN ensemble classifier," Fuzzy Systems and Knowledge Discovery (FSKD), 2012 9th International Conference on 29-31 May 2012, pp.297-301.

Method for 3D Image Representation with Reducing the Number of Frames based on Characteristics of Human Eyes

Kohei Arai[1]
Graduate School of Science and Engineering
Saga University
Saga City, Japan

***Abstract*—Method for 3D image representation with reducing the number of frames based on characteristics of human eyes is proposed together with representation of 3D depth by changing the pixel transparency. Through experiments, it is found that the proposed method allows reduction of the number of frames by the factor of 1/6. Also, it can represent the 3D depth through visual perceptions. Thus, real time volume rendering can be done with the proposed method.**

Keywords—3D image representation; Volume rendering; NTSC image display

I. Introduction

Computer input by human eyes only is proposed and implemented [1]-[3] together with its application to many fields, communication aids, electric wheel chair controls, having meal aids, information collection aids (phoning, search engine, watching TV, listening to radio, e-book/e-comic/e-learning/,etc., domestic helper robotics and so on [4]-[15]. In particular, the proposed computer input system by human eyes only does work like keyboard as well as mouse. Therefore, not only key-in operations but also mouse operations (right and left button click, drag and drop, single and double click) are available for the proposed system.

It is well known that hands, fingers operation is much slower than line of sight vector movements. It is also known that accidental blink is done within 0.3 second. Therefore, the proposed computer input system by human eyes only decides the specified key or location when the line of vector is fixed at the certain position of computer display for more than 0.3 second. In other words, the system can update the key or the location every 0.3 second. It is fast enough for most of all application fields. Meanwhile, 3D image display and manipulation can be done with 3D display. Attempts are also done with 2D display for 3D image display and manipulation [16],[17], on the other hands. Most of previous attempts are based on touch panel based manipulation by hands and fingers. As aforementioned, eyes operations are much faster than hands & fingers operations. Therefore, 3D image display and manipulation method by human eyes only is proposed in this paper.

3D image representations are widely used for a variety of applications such as medical electronics diagnostics image display, LSI pattern designs, and so on. Volume rendering is most popular method for 3D image representations, in general. It, however, takes a huge computational resources.

Volume rendering is in general costly. Real time representation, therefore, is not easy for volume rendering even for grid computing is used. For instance, 6 PCs of grid computing can be reduced by 35% of process time for the 3D representation with volume rendering. In order to reduce the process time of volume rendering, the number of frames which have to be display is reduced by using afterimage phenomenon. Time resolution of human eyes ranges from 50 to 100 ms. Illumination switching between on and off within the 50 to 100 ms is recognized as continuous illumination by human eyes. Therefore, it can be done to reduce the number of frames for 3D object image representation by using multi-layer representation. On the other hand, refresh cycle of the NTSC video signal corresponds to 33 ms. Therefore, the interval of refresh cycle has to be within 33 ms for the proposed volume rendering.

The next section describes the proposed system followed by experiment. Then concluding remarks are described with some discussions.

II. Proposed Method

A. Basic Idea

Basic Idea for the Proposed Method 3D model that displays a picture or item in a form that appears to be physically present with a designated structure. Essentially, it allows items that appeared flat to the human eye to be display in a form that allows for various dimensions to be represented. These dimensions include width, depth, and height. 3D model can be displayed as a two-dimensional image through a process called 3D rendering or used in a computer simulation of physical phenomena. The model can also be physically created using 3D printing devices. Models may be created automatically or manually. The manual modeling process of preparing geometric data for 3D computer graphics is similar to plastic arts such as sculpting.

There are some previously proposed methods for 3D display such as tracing object contour and reconstruct 3D object with line drawings, and wireframe representation and display 3D object with volume rendering. There is another method, so called OCT: Optical Coherence Tomography. It,

however, quit expensive than the others. Fundamental idea of the proposed method is afterimage. Response time of human eyes is that the time resolution of human eyes: 50ms～100ms. An afterimage or ghost image or image burn-in is an optical illusion that refers to an image continuing to appear in one's vision after the exposure to the original image has ceased. One of the most common afterimages is the bright glow that seems to float before one's eyes after looking into a light source for a few seconds. Afterimages come in two forms, negative (inverted) and positive (retaining original color). The process behind positive afterimages are unknown, though thought to be related to neural adaptation. On the other hand, negative afterimages are a retinal phenomenon and are well understood. Example of 3D image on to 2D display is shown in Fig.1. This is the proposed system concept. In the example, "A" marked 3D image of multi-fidus which is acquired with CT scanner is displayed onto computer screen. "B", "C", ... are behind it.

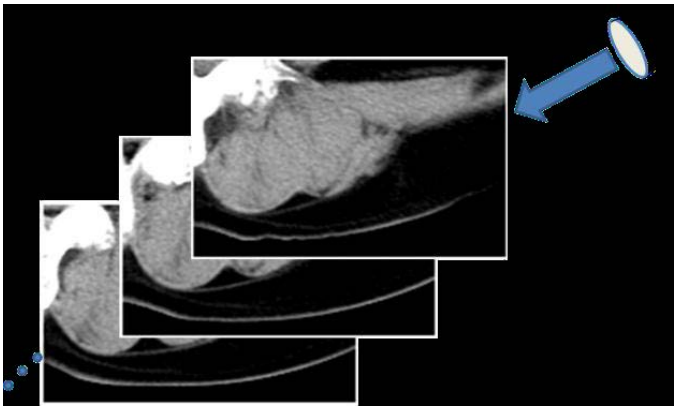

Fig. 1. System Concept

Such this layered 3D images are aligned with depth direction. Attached character "A" to "Z" are transparent and displayed at just beside the layered image at the different locations. Therefore, user can recognize the character and can select one of those characters by their eye. Arrow shows the line of sight vector. Curser can be controlled by human eyes only. By sweeping the character, 3D images are displayed by layer by layer. Therefore, it looks like time division delay of 3D images.

B. Displayed Image in Automatic Mode

Implementation of the proposed system is conducted. By using mouse operation by human eyes only, 3D image with different aspects can be recreated and display. It is confirmed that conventional image processing and analysis can be done with mouse operation by human eyes only.

Fig.2 shows the example of displayed layered images. In this example, 1024 of layer images are prepared for 3D object. By displaying the prepared layered images alternatively in automatic mode, 3D object appears on the screen. Furthermore, as shown in Fig.2, internal structure is visible other than the surface of the 3D object. It looks like a semitransparent 3D surface and internal structure in side of the 3D objects.

Another example is shown in Fig.3. In the figure, the first to 768th layer images are shown together with a slant view of the 3D object image with the several layer images. 1024 layer of images are created for the 3D object by using Open GL. Surface rendering with the 1024 layer of images makes a 3D object rendering like Fig.3.

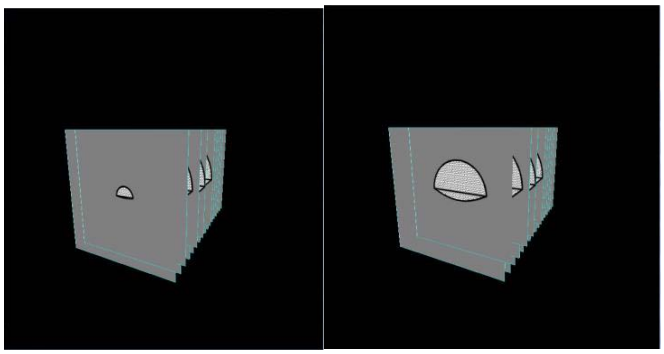

(a)#1 layer (b)#128 layer

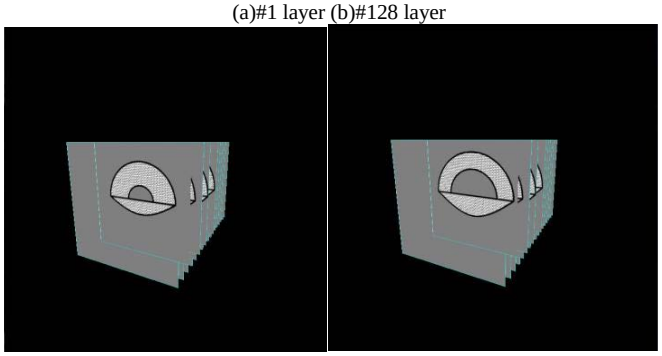

(c)#256 layer (d)#512 layer

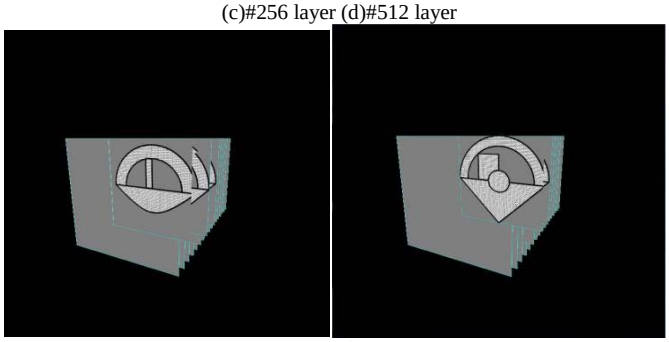

(e)#768 layer (f)#1024 layer

Fig. 2. Example of displayed layered images

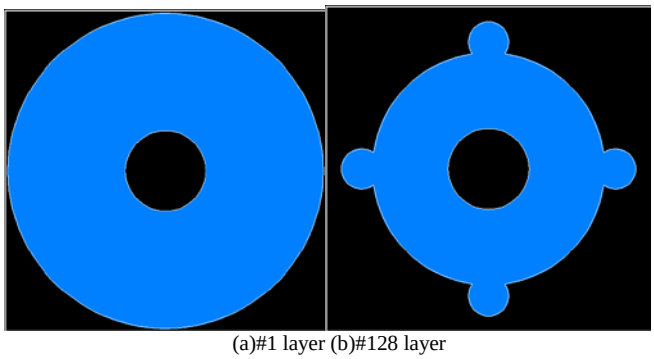

(a)#1 layer (b)#128 layer

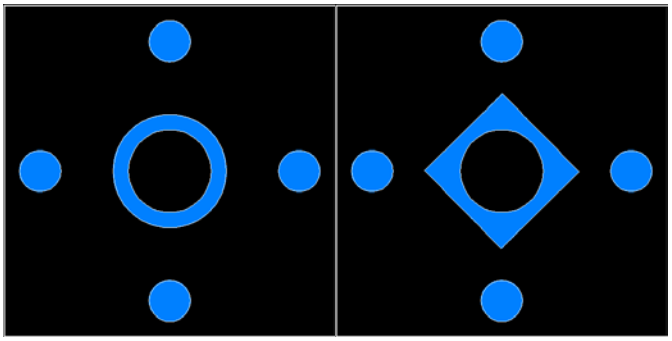

(c)#256 layer (d)#512 layer

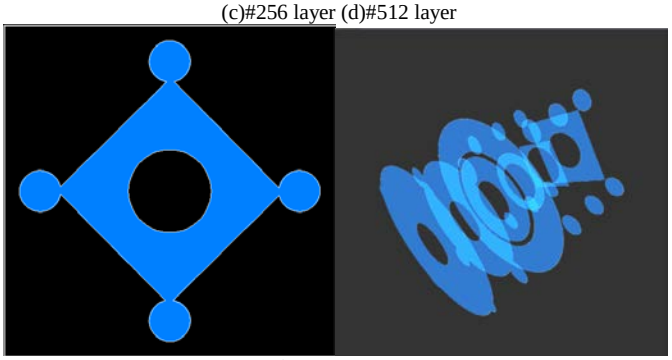

(e)#768 layer (f)several layer representation

Fig. 3. Example of 3D object image representation

Fig.4 shows the examples of 3D object representation images created with the 1024 layer of images which are shown in Fig.3 from the different aspects. There are ambiguities for the depth representation in the images of Fig.4. This is because of hidden line and surface distinguish process based on depth buffer method. Therefore, resultant image of the layer images surface rendering cannot represent 3D object properly which is shown in Fig.5.

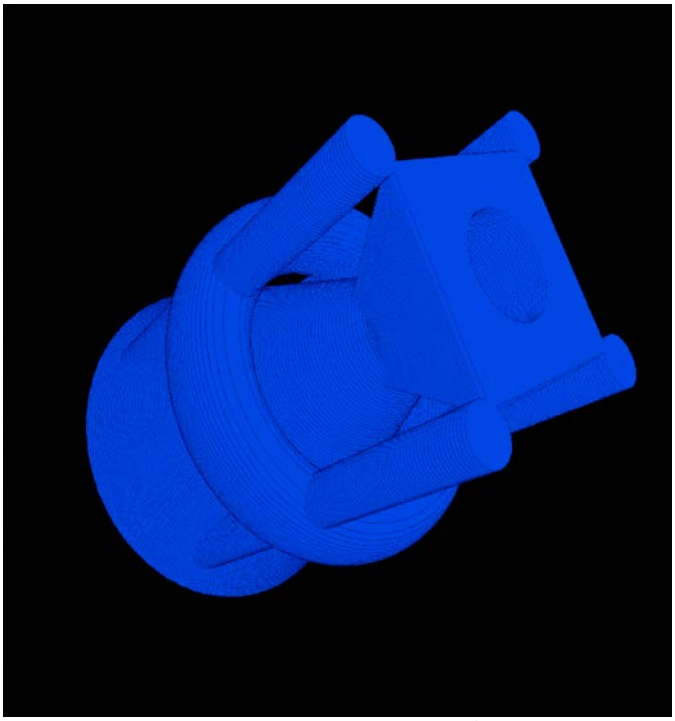

(a)3D object image representation (side view from the right)

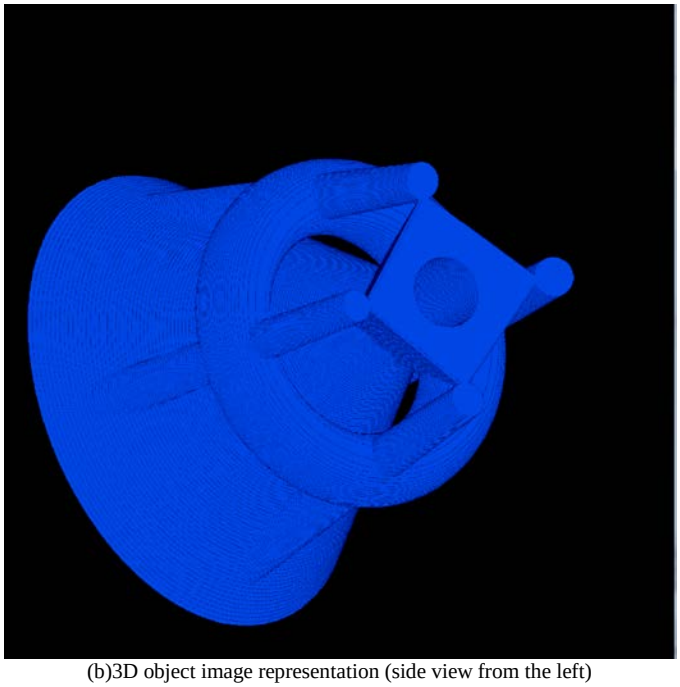

(b)3D object image representation (side view from the left)

Fig. 4. 3D object image representation from the different aspects

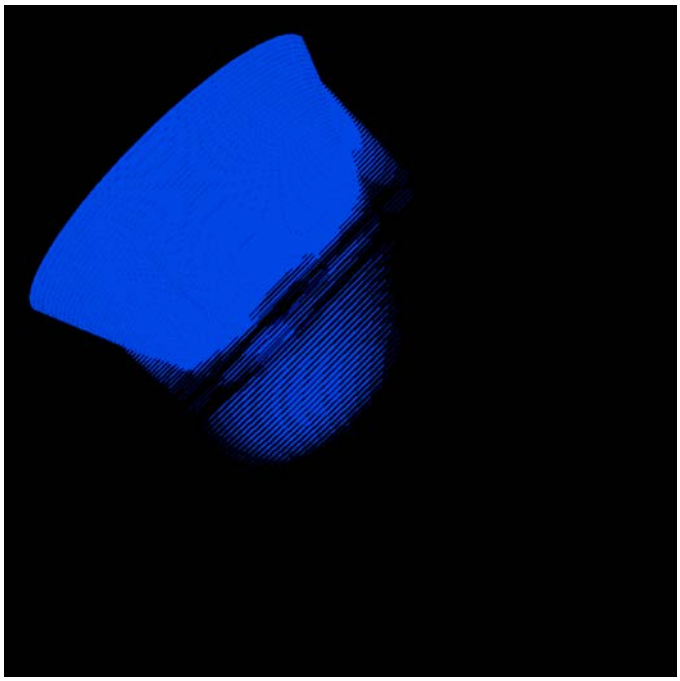

Fig. 5. 3D object image representation with hidden line and surface distinguish

C. Changing the Transparency

In order to represent the depth information, transparency is used. The purpose of the depth information representation is to express the internal structure of the 3D object. By changing the transparency, somewhat depth information can be represented as shown in Fig.6. In the figure, 100% denotes 0% transparent image while 5% also denotes 95% transparent image, respectively. It is clear that internal structure can be seen by changing transparency. Therefore, users can select the

transparency depending on which portion of internal structure would like to see through visual perception.

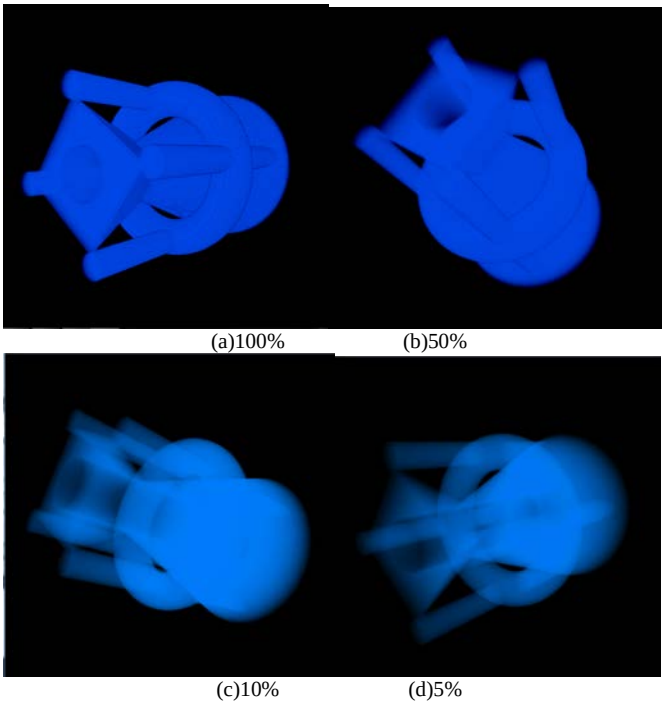

(a)100% (b)50%

(c)10% (d)5%

Fig. 6. Examples of 3D object image representation with changing transparency

D. Foggy Representation for Depth Representations

In order to represent the depth information, not only transparency but also foggy representation is added. Because of depth information representation is getting week depending on the transparency, it is needed to add some other representation for depth information. One of the effect is foggy representation with the different color.

(a)Fog added 3D image for depth representation

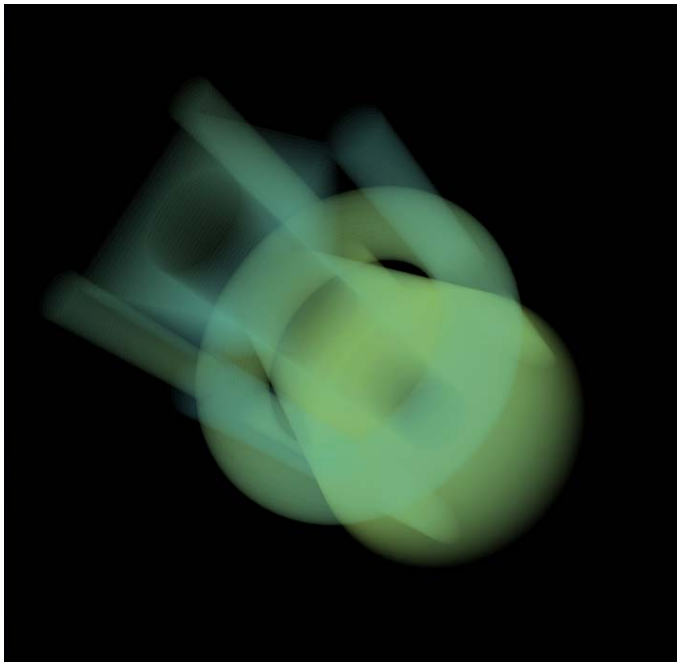

(b) Fog added 3D image for depth representation

Fig. 7. Examples of Fog added 3D image for depth representation

Fig.7 shows examples of foggy representation of depth information representations.

E. Implementation

Implementation is done based on Open GL. Parameter setting can be done with the slide ruler shown in Fig.8.

Fig. 8. Scroll slide bar for designation of parameters of 3D object image representations (the slide ruler is for the rotation angle in x axis followed by y and z axis and refresh cycle of the time interval of display as well as object frame interval ranges from 1 to 127

Slid rulers for rotation angles in x, y, and z axis which ranges from 0 to 355 degree, refresh cycle of time interval

which ranges from 1 to 100 ms, and object interval (the number of frames which ranges from 1 to 127) are available to set. The other parameter, such as transparency (ranges from 0 to 100 %), foggy representation can be set automatically.

As mentioned above, the time resolution of human eyes ranges from 50 to 100 ms. Illumination switching between on and off within the 50 to 100 ms is recognized as continuous illumination by human eyes. Therefore, it can be done to reduce the number of frames for 3D object image representation by using multi-layer representation. On the other hand, refresh cycle of the NTSC video signal corresponds to 33 ms. Therefore, the interval of refresh cycle has to be within 33 ms for the proposed volume rendering. Example of a frame image of the proposed volume rendering is shown in Fig.9.

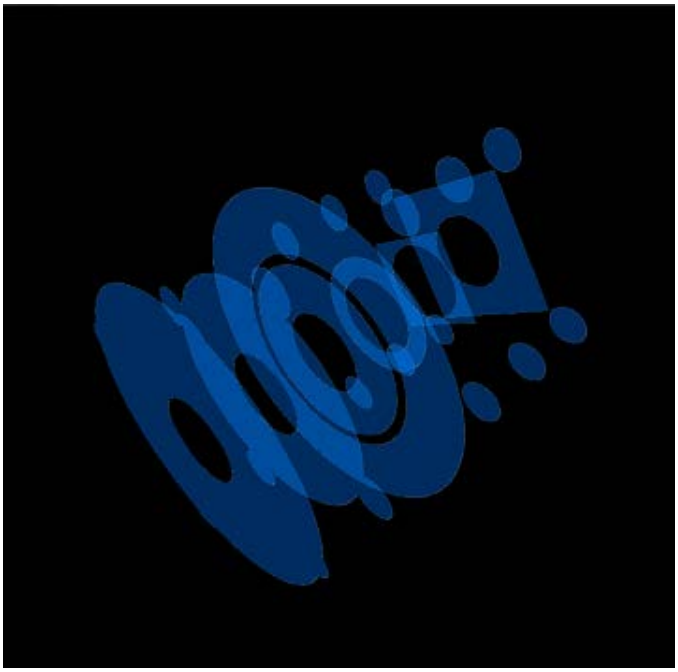

Fig. 9. Example of a frame image of the proposed volume rendering

III. EXPERIMENT

3D object image representation based on the proposed method with the image datasets used in this experiment were from the Laboratory of Human Anatomy and Embryology, University of Brussels (ULB), Belgium. Fig.10 shows examples of the resultant images. The 3D images used are derived from CT scan images. In these cases, the number of frames used is 127 while the transparency is set at 50 %. Meanwhile, the refresh cycle of the time interval is set at 17 ms which corresponds to 58 f/s. Thus, 1/6 of reduction can be achieved successfully.

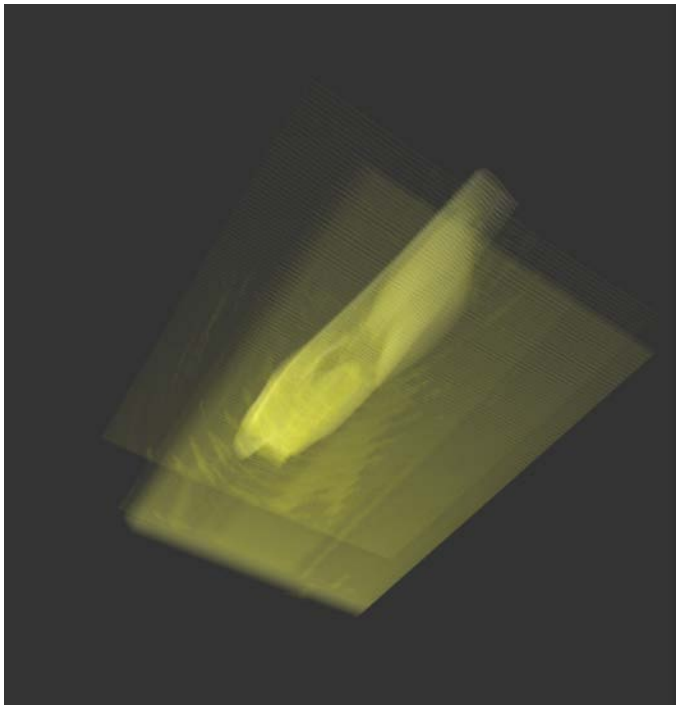

(a)Example #1

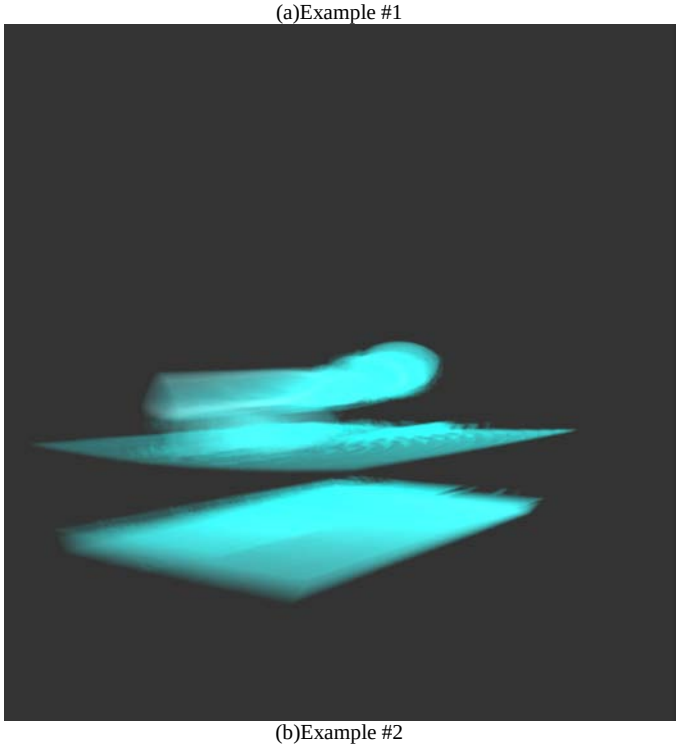

(b)Example #2

Fig. 10. 3D object image representation based on the proposed method with the image datasets used in this experiment were from the Laboratory of Human Anatomy and Embryology, University of Brussels (ULB), Belgium

IV. CONCLUSION

Method for 3D image representation with reducing the number of frames based on characteristics of human eyes is proposed together with representation of 3D depth by changing the pixel transparency. Through experiments, it is found that the proposed method allows reduction of the number of frames by the factor of 1/6. Also, it can represent the 3D depth through visual perceptions. Thus, real time representation of 3D object can be displayed onto computer screen.

Further investigations are required for improvement of frame reduction ratio. The refresh cycle has to be optimized. Also, the transparency and foggy representation has to be optimized. In other word, a method for optimization of the parameters has to be created.

REFERENCES

[1] K.Arai, H.Uwataki, Computer input by human eyes only based on cornea center extraction which allows users' movements, Journal of Institute of Electric Engineering of Japan, C-127, 7, 1107-1114, 2007.

[2] K.Arai, M.Yamaura, Improvement of blink detection performance based on Morphologic filter for computer input by human eyes only, Journal of Image Electronics Engineering Society of Japan, 37, 5, 601-609, 2008.

[3] K.Arai, K.Yajima, Communication aid based on computer input by human eyes only, Journal of Institute of Electric Engineering of Japan, C-128, 11, 1679-1686, 2008.

[4] D. Purwanto, R. Mardiyanto and K. Arai, Electric wheel chair control with gaze detection and eye blinking, Artificial Life and Robotics, AROB Journal, 14, 694,397-400, 2009.

[5] K.Arai, R. Mardiyanto, Computer input by human eyes only with blink detection based on Gabor filter, Journal of Visualization Society of Japan, 29,Suppl.2, 87-90,2009.

[6] K. Arai and R. Mardiyanto, Real time blinking detection based on Gabor filter, International Journal of Human Computer Interaction, 1, 3, 33-45, 2010.

[7] K. Arai and M. Yamaura, Computer input with human eyes only using two Purkinje images which works in a real time basis without calibration, International Journal of Human Computer Interaction, 1, 3, 71-82, 2010.

[8] K. Arai and R. Mardiyanto, Camera mouse and keyboard for handicap person with trouble shooting capability, recovery and complete mouse events, International Journal of Human Computer Interaction, 1, 3, 46-56, 2010.

[9] K. Arai, R. Mardiyanto, A prototype of electric wheel chair control by eye only for paralyzed user, Journal of Robotics and Mechatronics, 23, 1, 66-75, 2010.

[10] K. Arai, K. Yajima, Robot arm utilized having meal support system based on computer input by human eyes only, International Journal of Human-Computer Interaction, 2, 1, 120-128, 2011.

[11] Kohei Arai, Ronny Mardiyanto, Autonomous control of eye based electric wheel chair with obstacle avoidance and shortest path finding based on Dijkstra algorithm, International Journal of Advanced Computer Science and Applications, 2, 12, 19-25, 2011.

[12] K. Arai, R. Mardiyanto, Eye-based human-computer interaction allowing phoning, reading e-book/e-comic/e-learning, Internet browsing and TV information extraction, International Journal of Advanced Computer Science and Applications, 2, 12, 26-32, 2011.

[13] K. Arai, R. Mardiyanto, Eye based electric wheel chair control systemI(eye) can control EWC-, International Journal of Advanced Computer Science and Applications, 2, 12, 98-105, 2011.

[14] K. Arai, R. Mardiyanto, Evaluation of users' impact for using the proposed eye based HCI with moving and fixed keyboard by using eeg signals, International Journal of Research and Reviews on Computer Science, 2, 6, 1228-1234, 2011.

[15] K. Arai, R. Mardiyanto, Electric wheel chair controlled by human eyes only with obstacle avoidance, International Journal of Research and Reviews on Computer Science, 2, 6, 1235-1242, 2011

[16] K.Arai, X.Y.Guo, Method for 3D object of content representation and manipulations on 2D display using human eyes only, Proceedings of the International Conference on Convergence Content 2012, 49-50, 2012.

[17] Kohei Arai, Method for 3D rendering based on intersection image display which allows representation of internal structure of 3D objects, International Journal of Advanced Research in Artificial Intelligence, 2, 6, 46-50, 2013.

AUTHORS PROFILE

Kohei Arai, He received BS, MS and PhD degrees in 1972, 1974 and 1982, respectively. He was with The Institute for Industrial Science and Technology of the University of Tokyo from April 1974 to December 1978 and also was with National Space Development Agency of Japan from January, 1979 to March, 1990. During from 1985 to 1987, he was with Canada Centre for Remote Sensing as a Post Doctoral Fellow of National Science and Engineering Research Council of Canada. He moved to Saga University as a Professor in Department of Information Science on April 1990. He was a councilor for the Aeronautics and Space related to the Technology Committee of the Ministry of Science and Technology during from 1998 to 2000. He was a councilor of Saga University for 2002 and 2003. He also was an executive councilor for the Remote Sensing Society of Japan for 2003 to 2005. He is an Adjunct Professor of University of Arizona, USA since 1998. He also is Vice Chairman of the Commission-A of ICSU/COSPAR since 2008. He received Science and Engineering Award of the year 2014 from the minister of the ministry of Science Education of Japan and also received the Bset Paper Award of the year 2012 of IJACSA from Science and Information Organization: SAI. In 2016, he also received Vikram Sarabhai Medal of ICSU/COSPAR and also received 20 awards. He wrote 34 books and published 520 journal papers. He is Editor-in-Chief of International Journal of Advanced Computer Science and Applications as well as International Journal of Intelligent Systsems and Applications. http://teagis.ip.is.saga-u.ac.jp/

Sensitivity Analysis of Aerosol Parameter Estimations with Measured Solar Direct and Diffuse Irradiance

Kohei Arai[1]
Graduate School of Science and Engineering
Saga University
Saga City, Japan

***Abstract*—Sensitivity analysis of aerosol parameter (refractive index which consists of real and imaginary parts, size distribution which is represented by Junge parameter) estimations with measured solar direct and diffuse irradiance is made. Through experiments with the measured solar direct and diffuse irradiance, it is found that the results from the sensitivity analysis is valid and adequate.**

Keywords—Aerosol; Atmospheric optical depth; Solar irradiance; Solar direct; Solar diffuse; Aereole; Junge parameter; Size distribution; Real and imaginary parts of refractive index

I. Introduction

The largest uncertainty in estimation of the effects of atmospheric aerosols on climate systems is from uncertainties in the determination of their microphysical properties, including the aerosol complex index of refraction that in turn determines their optical properties. The methods, which allow estimation of refractive indices, have being proposed so far [1]-[3].

Most of the methods use ground based direct, diffuse and aureole measurement data such as AERONET [4] and SKYNET [5]. The methodology for estimation of a complete set of vertically resolved aerosol size distribution and refractive index data, yielding the vertical distribution of aerosol optical properties required for the determination of aerosol-induced radiative flux changes is proposed [6].

The method based on the optical constants determined from the radiative transfer models of the atmosphere is also proposed [7]. Laboratory based refractive indices estimation methods with spectral extinction measurements are proposed [8],[9]. All these existing methods are based on radiance from the sun and the atmosphere.

Through atmospheric optical depth measurements with a variety of relatively transparent wavelength, it is possible to estimate size distribution, molecule scattering, gaseous transmission, ozone and water vapor absorptions, etc. so that refractive index might be estimated [10]-[14]. In order to assess the estimation accuracy of refractive index with the proposed method, sensitivity analysis is conducted with a variety of parameters of the atmosphere. In particular, observation angle dependency is critical for atmospheric optical depth measurements. Therefore, it is conducted to assess influences due to observation angle on estimation accuracies of refractive index and size distribution. Similar researches are conducted and well reported [15]-[27].

The next section describes the proposed system followed by experiment. Then concluding remarks are described with some discussions.

II. Proposed Method

A. Radiative Transfer Function

Measured solar direct irradiance F on the ground is expressed in equation (1)

$$F = F_0 e^{-m_0 \tau_i} \quad (1)$$

where F_0 denotes extraterrestrial solar flux, m_0 denotes air-mass which can be represented as $1/\cos(\theta)$ where Θ denotes solar zenith angle, and τ_t denotes atmospheric optical depth which can be expressed in equation (2)

$$\tau_t = \tau_a + \tau_m = \tau_{as} + \tau_{aa} + \tau_{ms} + \tau_{ma} \quad (2)$$

where the first suffix *t*, *a* and *m* denotes total atmosphere, aerosols and molecules, respectively while the second suffix *a* and *s* denotes absorption and scattering, respectively. F can be measured on the ground while F_0 is well modeled by many researchers. On the other hand, m_0 can be well determined which results in estimation of atmospheric optical depth. Atmospheric optical depth due to aerosol and molecule has to be estimated together with their absorption and scattering components.

Meanwhile, measured solar diffuse irradiance on the ground can be expressed in equation (3).

$$E(\theta_0, \varphi) = E(\vartheta) = F m_0 \Delta\Omega \{\omega \tau_t P(\vartheta) + q(\vartheta)\} \quad (3)$$

where φ denotes the angle between solar azimuth and observation azimuth directions while ϑ denotes azimuth and elevation angles. There is the following relation between both angles,

$$\cos(\vartheta) = cos^2\theta_0 + sin^2\theta_0 cos\varphi \quad (4)$$

$\Delta\Omega$ denotes solid angle of the solar diffuse measuring instrument while ω denotes single scattering albedo which can be represented as follows,

$$\omega = (\tau_{as} + \tau_{ms})/\tau_{t_k} \quad (5)$$

$P(\vartheta)$ and $q(\vartheta)$ denotes scattering phase function and multiple scattering component, respectively. $P(\vartheta)$ is expressed as follows,

$$P(\vartheta) = \{\tau_{ms}P_m(\vartheta) + \tau_{as}P_a(\vartheta)\}/(\tau_{ms} + \tau_{as}) \quad (6)$$

Because of the observation wavelength and molecule radius has the following relation,

$$\frac{\pi r_a}{\lambda} < 0.4 \quad (7)$$

molecule component of scattering can be expressed based on the Rayleigh scattering theory. Molecule component of scattering phase function $P_m(\vartheta)$ can be expressed as follows,

$$P_m(\vartheta) = \left(\frac{3}{4}\right)(1 + cos^2\vartheta) \quad (8)$$

Molecule scattering component of the atmospheric optical depth is represented as follows,

$$\tau_{ms} = \{0.008569\lambda^{-4}(1 + 0.0113\lambda^{-2} + 0.00013\lambda^{-4})\}(\frac{p}{p_0})(\frac{T_0}{T}) \quad (9)$$

where λ denotes observation wavelength while p and p_0 denotes atmospheric pressure on the ground, standard atmospheric pressure (1013.25 hPa), respectively. On the other hand, T_0 and T denotes standard air-temperature on the ground (288.15 K) and air-temperature on the ground, respectively.

Meanwhile, observation wavelength and aerosol particle size has the following relation,

$$0.4 < \frac{\pi r_a}{\lambda} < 3 \quad (10)$$

Aerosol scattering is expressed based on the Mie scattering theory.

Aerosol scattering intensity is expressed as equation (11).

$$\beta_a(\vartheta) = \frac{r^2}{2\pi}\int_{r_{min}}^{r_{max}}\{i_1(\vartheta, x, \tilde{m}) + i_2(\vartheta, x, \tilde{m})\}n(r)dr \quad (11)$$

where i1, i2 denotes Mie scattering intensity function as the function of x of size parameter, ϑ, and $\tilde{m}$ of aerosol refractive index. On the other hand, *n(r)* denotes the number of aerosol particles of which the radius is *r* and is called as number of aerosol particle size distribution in unit of 1/cm^2/μm.

$$\mathrm{n(r)} = \mathrm{dN(r)/dr} \quad (12)$$

The size parameter can be represented as follows,

$$\mathrm{x} = \left(\frac{2\pi}{\lambda}\right)r \quad (13)$$

On the other hand, aerosol optical depth is represented as follows,

$$\tau_a = \int_{r_{min}}^{r_{max}}\pi r^2 Q_{ext}(x, \tilde{m})n(r)dr \quad (14)$$

where Q is called as Extinction Efficiency Factor. Sometime, the following volume scattering size distribution is used.

$$\mathrm{v(r)} = \frac{vd}{d\ln r} \quad (15)$$

There is the well-known relation between the number and volume of size distributions as follows,

$$\mathrm{v(r)} = \frac{4}{3}\pi r^4 n(r) \quad (16)$$

Junge proposed the following size distribution function with Junge parameter γ,

$$\mathrm{C}r^{-\gamma} = \frac{dn}{d\ln r} \quad (17)$$

In this paper, the Junge function of size distribution is used because of its simplicity with only one Junge parameter.

Let integral kernel functions be

$$K_{ext}(x, \tilde{m}) = \left(\frac{3}{4}\right)\frac{Q_{ext}(x,\tilde{m})}{x}$$
$$\mathrm{K}(\vartheta, \mathrm{x}, \widetilde{m}) = \frac{3}{2}\frac{i_1(\vartheta,x,\tilde{m}) + i_2(\vartheta,x,\tilde{m})}{x^3} \quad (18)$$

Then

$$\beta_a(\vartheta) = \frac{2\pi}{\lambda}\int_{r_{min}}^{r_{max}} K(\vartheta, x, \tilde{m})v(r)\, d\ln\, r \quad (19)$$

$$\tau_a = \frac{2\pi}{\lambda}\int_{r_{min}}^{r_{max}} K_{ext}(x, \tilde{m})v(r)\, d\ln \quad r \quad (20)$$

$$P_a(\vartheta) = \beta_a(\vartheta)/\omega_a\tau_a \quad (21)$$

Solar diffuse irradiance taking into account the multiple scattering in the atmosphere measured on the ground can be represented as follows,

$$\mathrm{L}(\vartheta) = F_0 m_0 e^{-m\tau_t}\{(\tau_{ms} + \tau_{MS})P_m(\vartheta) + \tau_{as}P_a(\vartheta) + \tau_A P_m(0°)\} \quad (22)$$

where $(\tau_{ms}P_m(\vartheta))$ implies Rayleigh scattering component while $(\tau_{MS})P_m(\vartheta)$ implies multiple scattering component in the atmosphere. On the other hand, $\tau_{as}P_a(\vartheta)$ implies aerosol scattering component while $\tau_A P_m(0°)$ implies multiple scattering component in the atmosphere after the reflection on the ground. Solar diffuse flux can be expressed as L(ϑ) multiplied by observation solid angle $\Delta\Omega$. Meanwhile, $\tau_{MS}$and τ_A are expressed empirically as follows,

$$\tau_{MS} = 0.02\tau_{SS} + 1.2\tau_{SS}^2\mu_0^{\frac{-1}{4}} \quad (23)$$

$$\tau_A = \frac{A\tau_2}{1 - A\tau_3} \quad (24)$$

where

$$\tau_{SS} = \tau_{ms} + \tau_{sa}$$
$$\mu_0 = \cos(\theta_0)$$
$$\tau_2 = 1.34\tau_{SS}\mu_0\{1 + 0.22\left(\frac{\tau_{SS}}{\mu_0}\right)^2\}$$
$$\tau_3 = 0.9\tau_S - 0.92\tau_{SS}^2 + 0.54\tau_{SS}^3$$

Therefore, the contribution of multiple scattering in the atmosphere is expressed as follows,

$$\mathrm{q}(\vartheta) = \tau_{MS}P_m(\vartheta) + \tau_A P_m(0°) \quad (25)$$

B. Actual Radiative Transfer Equation Solving

The following much stable parameter is introduced,

$$R(\vartheta) = \frac{E(\vartheta)}{Fm_0\Delta\Omega} = \omega\tau_t P(\vartheta) + q(\vartheta) = \beta(\vartheta) + q(\vartheta) \quad (26)$$

Instead of $E(\vartheta)$, $R(\vartheta)$ does not have large influence due to calibration error of the measuring instrument for solar direct and diffuse irradiance. $\omega\tau_t P(\vartheta)$ is replaced to $\beta(\vartheta)$. It is called single scattering intensity. Widely used aerosol parameter estimation method and software code is called Skyrad.Pack developed by Teruyuki Nakajima [11]. In the Skyrad.Pack ver.4.2, iteration method is used as follows,

$$\beta_a^{(1)}(\vartheta) = R_{mean}(\vartheta)$$
$$\beta_a^{(n+1)}(\vartheta) = R_{mean}(\vartheta)\,\beta_a^{(n)}(\vartheta)\Big/_{R^{(n)}}(\vartheta)$$

where (n) denotes the iteration number while $R_{mean}(\vartheta)$ denotes the measured solar diffuse irradiance. This method is appropriate in the sense of optimization of single scattering albedo and flux, as well as contribution factor of the multiple scattering component. In order to estimated single scattering flux, we have to know aerosol refractive index and size distribution. Therefore, inverse problem solving method is needed for this. The proposed method uses Moore-Penrose generalized inverse matrix method. Volume vector v (r dimension) of unknown size distribution $v^{(n)}(r)$ is assumed to be the matrix g which consists of a measured aerosol scattering flux $\beta_a^{(n)}(\vartheta)$ and aerosol optical depth $\tau_a^{(n-1)}$. Then,

$$g = Gv \quad + \varepsilon \tag{27}$$

where G denotes a linear multiple term matrix. Thus, the size distribution can be determined as follows,

$$v = (G^T G + \eta H)^{-1} A^T g \tag{28}$$

where H denotes a smoothing matrix while η denotes Lagrange multiplier.

III. Experiments

A. The Instrument and Data Used

POM-01 of sky-radiometer which allows measurements of solar direct and diffuse as well as aureole irradiance measurements is used. Fig.1 shows outlook and calibration coefficient trend of the POM-1. POM-01 is set up on the top of the 7th building of the Science and Engineering Faculty of Saga University (1 Honjo, Saga, 840-8502 Japan). POM-01 measures solar direct irradiance with sun tracking capability and solar diffuse irradiance with 50 different diffuse angles in maximum with the following 7 center wavelength, 315, 400, 500, 675, 870, 940, 1020 nm. 315 nm is ozone absorption band while 940 nm is water absorption band, respectively.

(a)Outlook

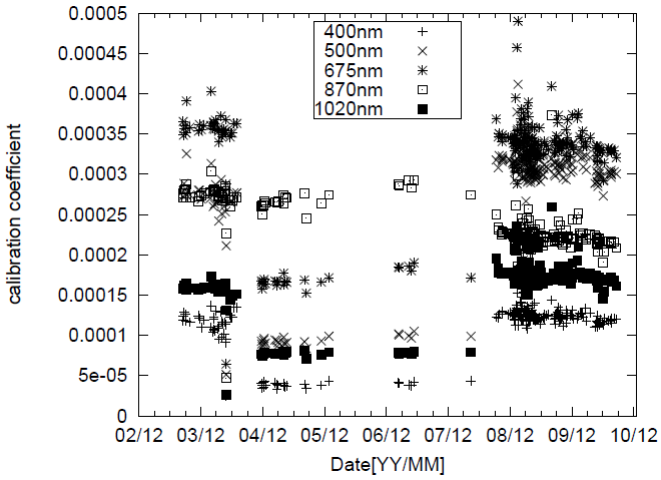

(b)Calibration coefficient

Fig. 1. Outlook and calibration coefficient trend of POM-01

POM-01 has self-calibration function. Using the function, calibration data is acquired routinely. Calibration coefficient trend can be divided into three periods, March 2003 to July 2004, July 2004 to October 2008, and October to now.

Fine weather condition of sky-radiometer data which is measured at 11:08 in the morning on May 25 2009 in the third period is selected due to the fact that calibration coefficients in the third period is relatively stable.

B. The Preliminary Experiments

The measured data for both solar direct and diffuse irradiances are in unit of output power. Firstly, the measured output powers are plotted as a function of scattering angle with the percent error of the solar direction in Fig.2. In accordance with increasing of solar direct angle error, the output power of POM-01 is getting down as shown in Fig.2 (a). Meanwhile, the output power of POM-01 decreases in accordance with increasing of solar diffuse angle error as shown in Fig.2 (b).

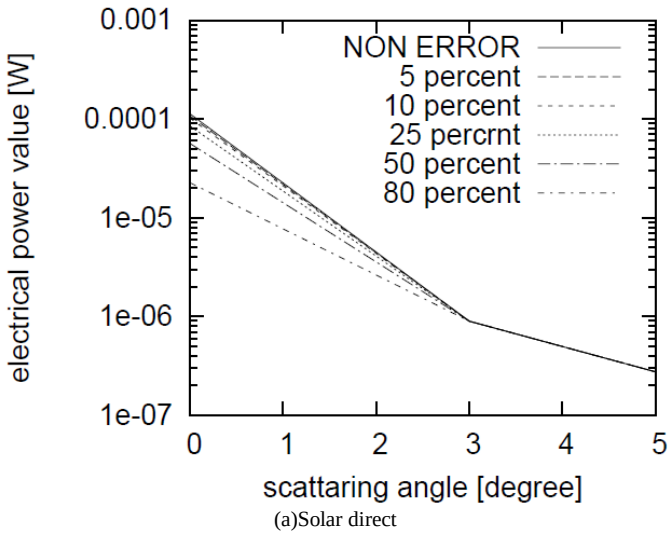

(a)Solar direct

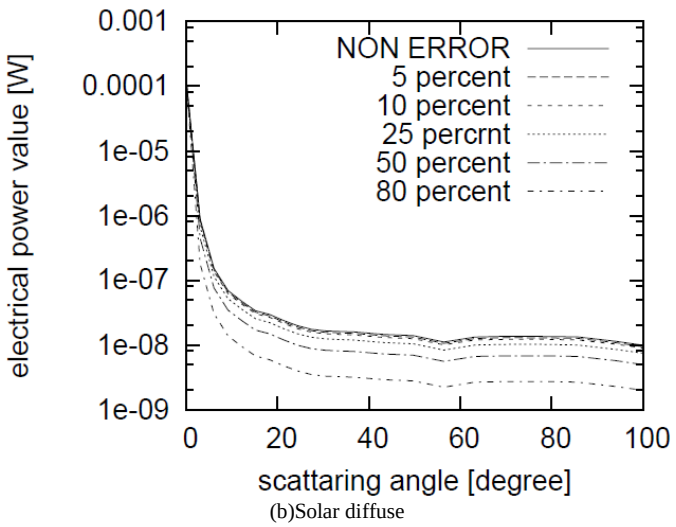

(b)Solar diffuse

Fig. 2. POM-01 output power with pointing error on solar directions

On the other hand, skyrad.pack ver.4.2 allows estimation of volume spectral aerosol size distribution function. Using the relation between volume spectra and Junge size distribution function, equation (16), Junge parameter can be estimated based on the well-known least square method. Fig.3 shows the estimated Junge size distribution function for the aerosols on May 25 2009. It is found that the least square method does works for conversion from volume spectra to Junge distribution function with quit small error.

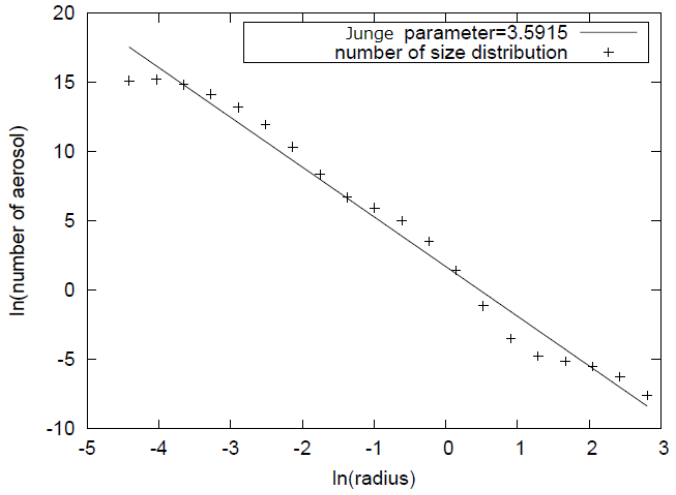

Fig. 3. Junge size distribution function of the aerosols on May 25 2009

The skyrad.Pack ver.4.2 requires the parameter for conversion, the number of iterations (NLOOP). In order to determine the parameter, the residual error is calculated as a function of NLOOP for the data which is acquired on May 25 2009. Fig. 4 shows the result. Fig.4 also shows the approximate function of residual errors which is expressed with the following function,

$$f(x) = ax^b \quad (29)$$

where a = 397.708 and b = -1.602.

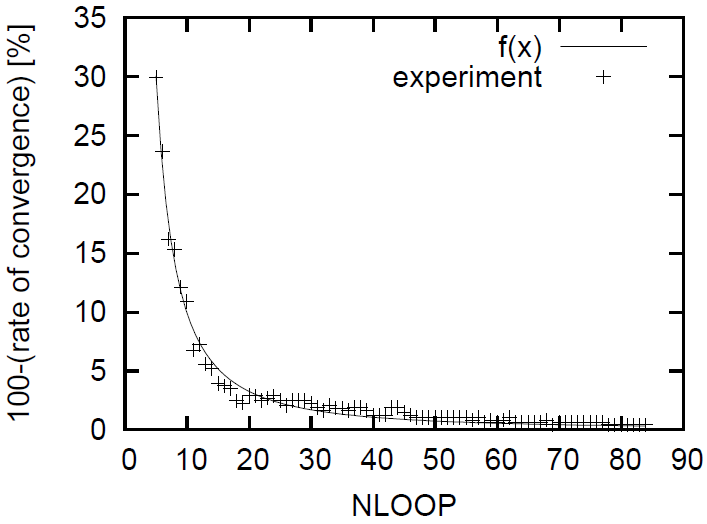

Fig. 4. Residual error (100-rate of c0nversgence) as the function of the number of iterations (NLOOP)

C. The Experimental Results

Using the modified skyrad.pack ver.4.2 described above, aerosol parameters, Real and Imaginary parts of aerosol refractive index and size distribution (Junge parameter) are estimated with the measured solar direct and diffuse irradiance which are measured with POM-01 on May 25 2009. Some of the errors are added on the solar direct angle and solar diffuse angle, respectively. Thus sensitivities of the pointing angle error on the estimated aerosol parameters are clarified.

Fig.5 shows the solar direct pointing angle error on the estimated real part of refractive index. The estimation error is evaluated with Root Mean Square Error: RMSE and percent error. As shown in Fig.5 (a) and (b), it is easily found that both of RMSE and percent error increases in accordance with increasing of solar direct pointing angle error. Also, it is found that both of RMSE and percent error increases in accordance with decreasing of wavelength.

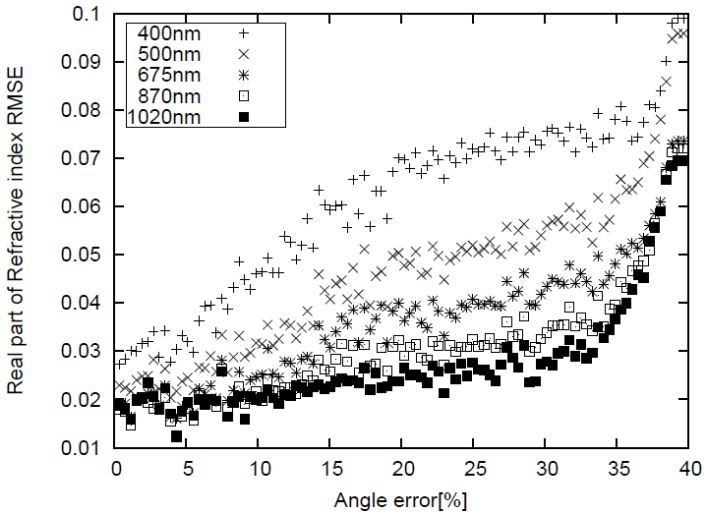

(a)RMSE

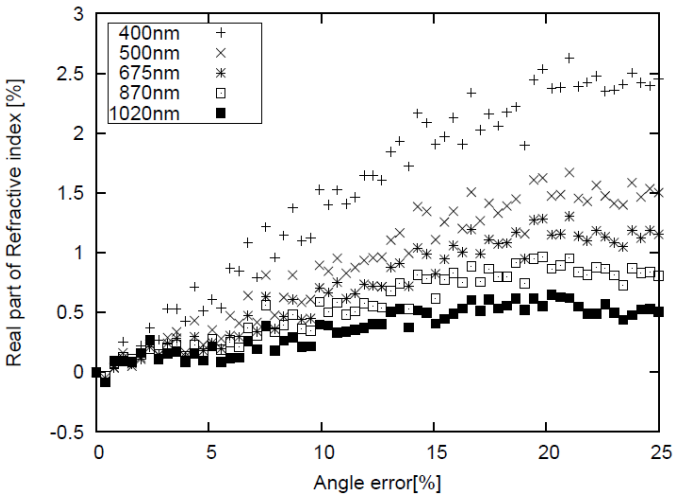

(b) Percent Error

Fig. 5. RMSE and percent error of real part of refractive index caused by the solar direct angle error

On the other hand, Fig.6 shows the solar direct pointing angle error on the estimated imaginary part of refractive index. As shown in Fig.6 (a) and (b), it is easily found that both of RMSE and percent error increases in accordance with increasing of solar direct pointing angle error. Also, it is found that both of RMSE and percent error increases in accordance with decreasing of wavelength. RMSE and percent error of estimation error for real part of refractive index is much greater than that for imaginary part of refractive index obviously. Also, solar direct pointing angle error dependency on real part of refractive index is much smooth in comparison to that on imaginary part of refractive index. In other word, the estimated imaginary part of refractive index is much diverse than the estimated real part of refractive index. This is because of the actual real part of refractive index is much greater than that of imaginary part of refractive index.

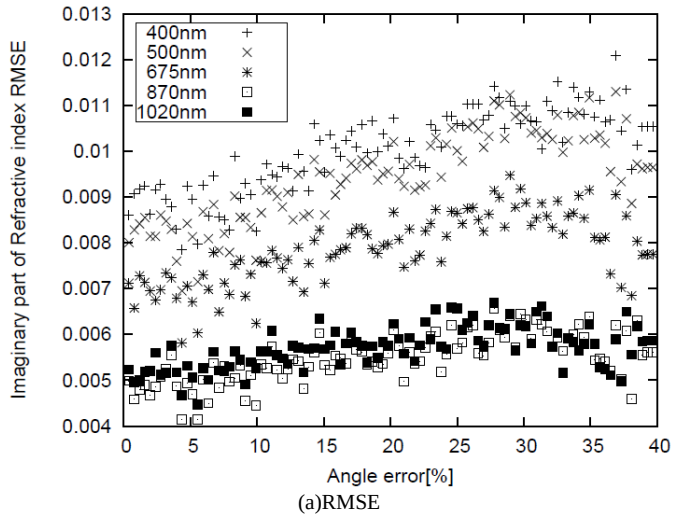

(a)RMSE

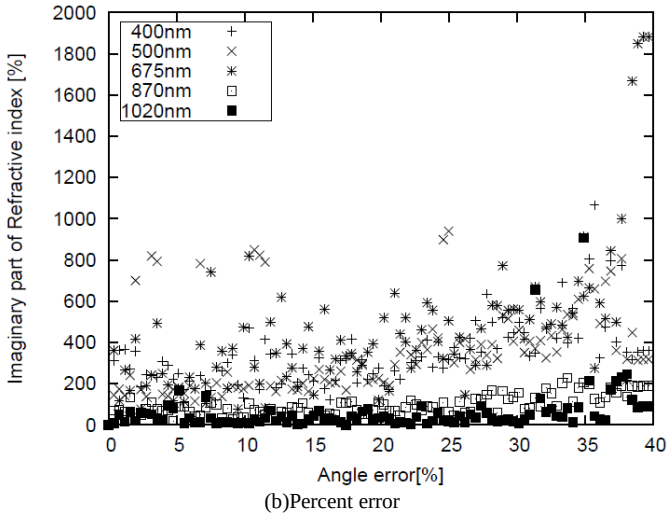

(b)Percent error

Fig. 6. RMSE and percent error of imaginary part of refractive index caused by solar diffuse angle error

Furthermore, it is found that RMSE of Junge parameter increases with increasing of solar direct pointing error as shown in Fig.7.

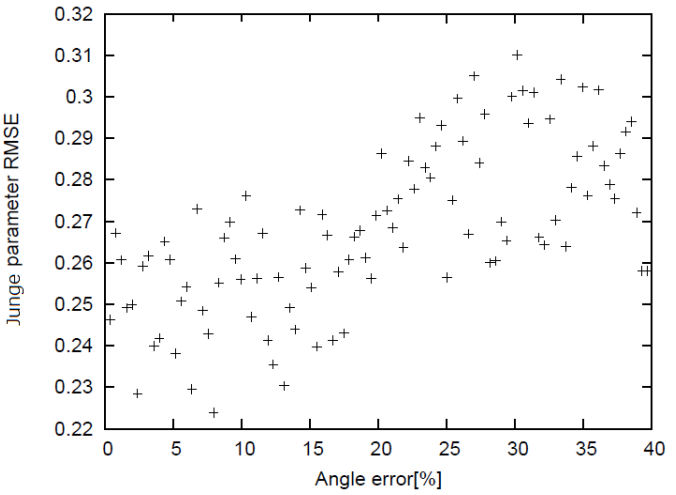

Fig. 7. RMSE of Junge parameter with the changing of solar direct pointing angle error

Meanwhile, Fig.8 (a) and (b) shows the solar diffuse pointing angle error on RMSE and percent error of the estimated real part of refractive index, respectively. As shown in Fig.8 (a) and (b), it is easily found that both of RMSE and percent error increases in accordance with increasing of solar diffuse pointing angle error. Also, it is found that both of RMSE and percent error increases in accordance with decreasing of wavelength.

On the other hand, Fig.9 shows the solar diffuse pointing angle error on the estimated imaginary part of refractive index.

As shown in Fig.9 (a) and (b), it is easily found that both of RMSE and percent error increases in accordance with increasing of solar diffuse pointing angle error. Also, it is found that both of RMSE and percent error increases in accordance with decreasing of wavelength. RMSE and percent error of estimation error for real part of refractive index is much greater than that for imaginary part of refractive index obviously. Also, solar diffuse pointing angle error dependency on real part of refractive index is much smooth in comparison to that on imaginary part of refractive index.

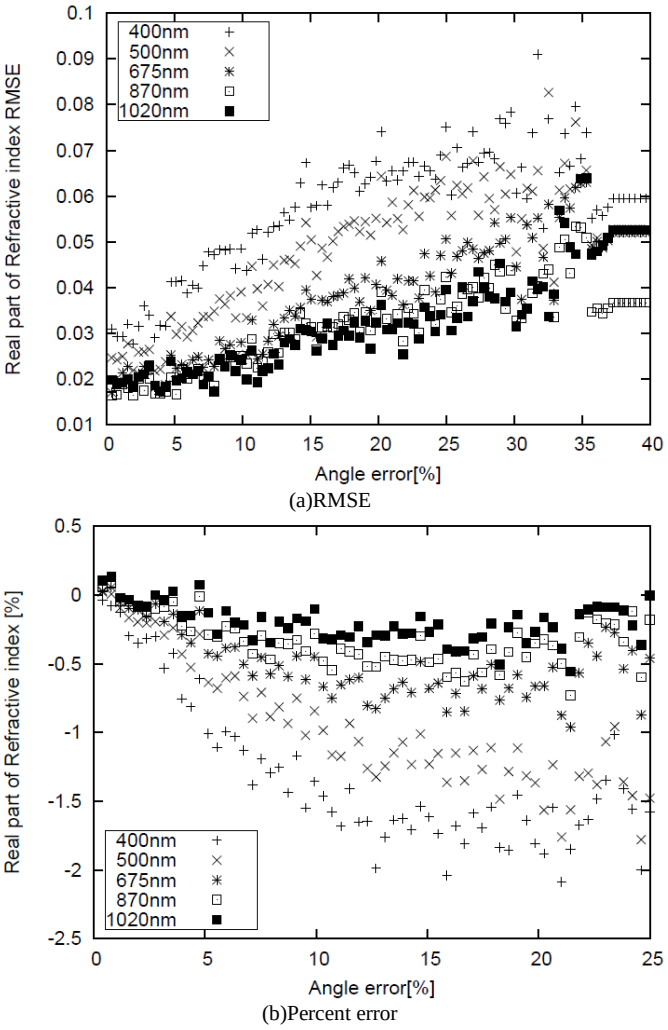

Fig. 8. RMSE and percent error of real part of refractive index caused by solar diffuse angle error

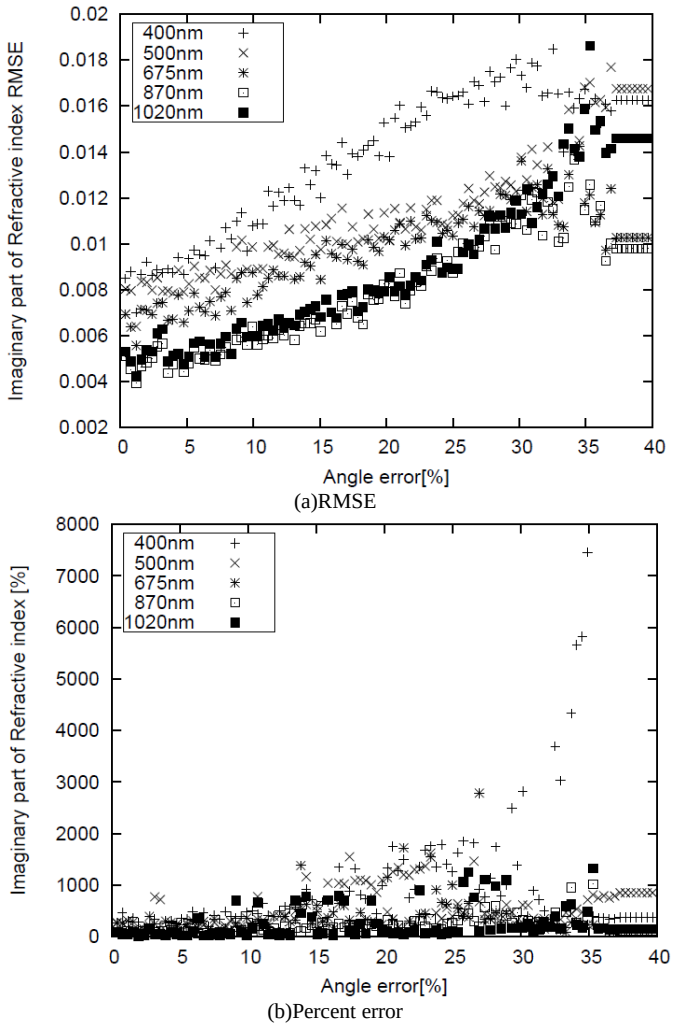

Fig. 9. RMSE and percent error of imaginary part of refractive index caused by solar diffuse angle error

In other word, the estimated imaginary part of refractive index is much diverse than the estimated real part of refractive index. This is because of the actual real part of refractive index is much greater than that of imaginary part of refractive index.

Furthermore, it is found that RMSE of Junge parameter increases with increasing of solar direct pointing error as shown in Fig.10.

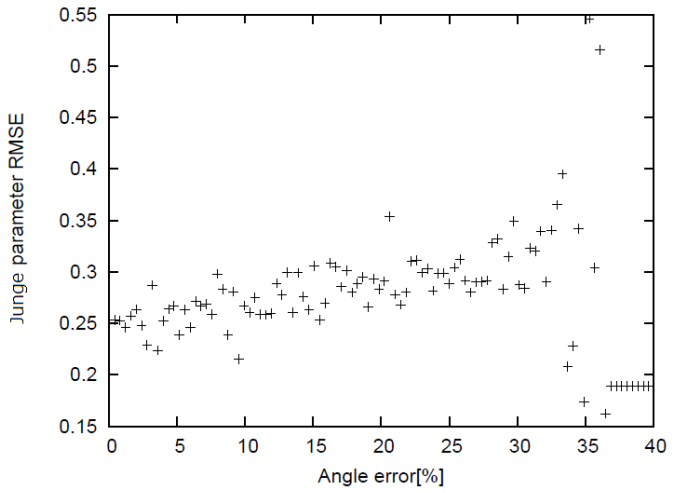

Fig. 10. RMSE of Junge parameter with the changing of solar diffuse pointing angle error

IV. Conclusion

Sensitivity analysis of aerosol parameter (refractive index which consists of real and imaginary parts, size distribution which is represented by Junge parameter) estimations with measured solar direct and diffuse irradiance is made. Through experiments with the measured solar direct and diffuse irradiance, it is found that the real part of refractive index estimation RMS error ranges from 0.01 to 0.035 which corresponds to 0.1 to 0.7 % error while RMSE of imaginary part of refractive index ranges from 0.004 to 0.0092 for less than 5 degree of the solar direct pointing angle error. On the other hand, it is also found that RMSE of the Junge parameter estimation error ranges from 0.22 to 0.269 for less than 5 degree of the solar direct pointing angle error.

Furthermore, it is found that the real part of refractive index estimation RMS error ranges from 0.017 to 0.036 which corresponds to 0.1 to 1.2 % error while RMSE of imaginary part of refractive index ranges from 0.004 to 0.0095 for less than 5 degree of the solar diffuse pointing angle error. On the other hand, it is also found that RMSE of the Junge parameter estimation error ranges from 0.23 to 0.29 for less than 5 degree of the solar diffuse pointing angle error. Therefore, pointing angle accuracy requirement for solar diffuse irradiance is little bit higher than that for solar direct irradiance.

Further investigations are required for the sensitivity analysis with the different characteristics of error (random number), not only for the uniformly distributed random number (this is used in this paper) but also the chi-square distribution of random number of error is taken into account.

Acknowledgements

Author would like to thank Mr. Yu Odeishi of former student of Saga University for his effort for conducting the experiments.

References

[1] Shaw, G.E., Error analysis of multi-wavelength sunphotometry. Pure Appl. Geophys., 114, 1, 1976.

[2] Hoppel, W. A., J. W. Fitzgerald, G. M. Frick, R. E. Larson, and E. J. Mack, Aerosol size distributions and optical properties found in the marine boundary layer over the Atlantic Ocean, J. Geophys. Res., 95, 3659-3686, 1990.

[3] Holben, B. N., et al., AERONET- A federated instrument network and data achieve for aerosol characterization, Remote Sens., 12, 1147-1163, 1991.

[4] Holben, B.N., and Coauthors, AERONET-A federated instrument network and data archive for aerosol characterization. Remote Sens. Environ., 66, 1-16. 1998.

[5] Aoki, K., T. Takamura, and T. Nakajima, Aerosol optical properties measured by SKYNET sky radiometer validation network. Proc. of the 2nd EarthCARE Workshop, 133-134, 2005.

[6] Redemann, R. P. Turco, K. N. Liou, P. B. Russell, R. W. Bergstrom, B. Schmid, J. M. Livingston, P. V. Hobbs, W. S. Hartley, S. Ismail, R. A Ferrare, E. V. Browell, Retrieving the vertical structure of the effective aerosol complex index of refraction from a combination of aerosol in situ and remote sensing measurements during TARFOX, J. Geophys. Res., 105, D8, 9949–9970, 2000.

[7] M.L.Clapp, and R.E.Miller, Complex Refractive Indices of Crystalline Hydrazine from Aerosol Extinction Spectra, Icarus, 23, 2, 396-403(8), 1996.

[8] R. Eiden, Determination of the complex index of refraction of spherical aerosol particles, Appl. Opt. 10, 749-757, 1971.

[9] G. E. Thomas, S. F. Bass, R. G. Grainger, and A. Lambert, Retrieval of aerosol refractive index from extinction spectra with a damped harmonic-oscillator band model, Appl. Opt. 44, 1332-1341, 2005.

[10] Kohei Arai, Aerosol refractive index retrievals with atmospheric polarization measuring data, Proceedings of the SPIE, 7461-06, 1-9, 2009

[11] Teruyuki Nakajima, et al., Use of sky brightness measurements from ground for remote sensing of particulate polydispersions, Applied Optics, Vol.35 No..15 pp.2672-2686 May 1996.

[12] Teruyuki Nakajima, et al., Retrieval of the optical properties of aerosols from aureole and extinction data, Applied Optics, Vol.22 No..19 pp.2951-2959 October 1983.

[13] M. A. Box and A. Deepak, An Approximation to Multiple Scattering in the Earth's Atmo-sphere:Almucanter Radiance Formulation, J. Atmos. Sci. Vol38 pp.1037-1048 1981.

[14] Mitsugu Toriumi, Hideaki Takenaka, Tadashi Kato, Toshikazu Hasegawa, Takashi Nakajima, Tamio Takamura and Teruyuki Nakajima: Estimation of Aerosol Optical Thickness by PAR Radiometer, Journal of The Remote Sensing Society of Japan, 30, 2, pp.81-89, 2010 .

[15] Tsutomu Takashima, Kazuhiko Masuda, Kohei Arai, Satoshi Tsuchida, Observation of Optical Property of the Atmosphere in Particular Aerosols at Deserted Areas In USA Using Sun-photometer and Polarization Spectrometer, Journal of Remote Sensing Society of Japan, Vol.20, No.3, pp.47-60, (2000).

[16] Kohei Arai, Influence of Non-Spherical Sea Salt Aerosol Particles Containing Bubbles on the Top of the Atmosphere Radiance, Journal of Remote Sensing Society of Japan, Vol.20, No.5, pp.32-39, (2001).

[17] Kohei Arai, Tatsuya Kawaguchi, Adjucency Effect of Layered Clouds taking Into Account Phase Function of Cloud Particles and Multi-Layered Plane Parallel Atmosphere Based on Monte Carlo Method, Journal of Japan Society of Photogrammetry and Remote Sensing, Vol.40, No.6, 2001.

[18] Kohei Arai, Yoko Takamatsu, Influence of Spume Aerosol Particles on the Top of the Atmosphere Radiance, Journal of Remote Sensing Society of Japan, Vol.23, No.4, pp.355-363, 2003.

[19] Kohei Arai, Xing Ming Liang, Estimation of Method for the Top of the Atmosphere Radiance Taking Into Account Polarized Up-welling and Down-welling Radiance, Journal of Japan Society of Photogrammetry and Remote Sensing, 44,3, 4-12,(2005)

[20] K.Arai, Monte Carlo simulation of polarized atmospheric irradiance for determination of refractive index of aerosols, International Journal of Research and Review on Computer Science, 3, 4, 1744-1748, 2012.

[21] K.Arai, Monte Carlo ray tracing based sensitivity analysis of the atmospheric and oceanic parameters on the top of the atmosphere radiance, International Journal of Advanced Computer Science and Applications, 3, 12, 7-13, 2012.

[22] K.Arai, Monte Carlo ray tracing based sensitivity analysis of the atmospheric and oceanic parameters on the top of the atmosphere radiance, International Journal of Advanced Computer Science and Applications, 3, 12, 7-13, 2012.

[23] Kohei Arai, Method for estimation of aerosol parameters based on ground based atmospheric polarization irradiance measurements, International Journal of Advanced Computer Science and Applications, 4, 2, 226-233, 2013.

[24] Kohei Arai, Sensitivity analysis and validation of refractive index estimation method with ground based atmospheric polarized radiance measurement data, International Journal of Advanced Computer Science and Applications, 4, 3, 1-6, 2013.

[25] Kohei Arai, Sensitivity analysis for aerosol refractive index and size distribution estimation methods based on polarized atmospheric irradiance measurements, International Journal of Advanced Research in Artificial Intelligence, 3, 1, 16-23, 2014.

[26] K.Arai, Vicarious calibration data screening method based on variance of surface reflectance and atmospheric optical depth together with cross calibration, International Journal of Advanced Research on Artificial Intelligence, 4, 11, 1-8, 2015.

[27] K.Arai, Kenta Azuma, Method for surface reflectance estimation with MODIS by means of bi-section between MODIS and estimated radiance as well as atmospheric correction with sky-radiometer, International Journal of Advanced Research on Artificial Intelligence, 4, 11, 8-15, 2015.

AUTHORS PROFILE

Kohei Arai, He received BS, MS and PhD degrees in 1972, 1974 and 1982, respectively. He was with The Institute for Industrial Science and Technology of the University of Tokyo from April 1974 to December 1978 and also was with National Space Development Agency of Japan from January, 1979 to March, 1990. During from 1985 to 1987, he was with Canada Centre for Remote Sensing as a Post Doctoral Fellow of National Science and Engineering Research Council of Canada. He moved to Saga University as a Professor in Department of Information Science on April 1990. He was a councilor for the Aeronautics and Space related to the Technology Committee of the Ministry of Science and Technology during from 1998 to 2000. He was a councilor of Saga University for 2002 and 2003. He also was an executive councilor for the Remote Sensing Society of Japan for 2003 to 2005. He is an Adjunct Professor of University of Arizona, USA since 1998. He also is Vice Chairman of the Commission-A of ICSU/COSPAR since 2008. He received Science and Engineering Award of the year 2014 from the minister of the ministry of Science Education of Japan and also received the Bset Paper Award of the year 2012 of IJACSA from Science and Information Organization: SAI. In 2016, he also received Vikram Sarabhai Medal of ICSU/COSPAR and also received 20 awards. He wrote 34 books and published 520 journal papers. He is Editor-in-Chief of International Journal of Advanced Computer Science and Applications as well as International Journal of Intelligent Systsems and Applications. http://teagis.ip.is.saga-u.ac.jp/

Information-Theoretic Active SOM for Improving Generalization Performance

Ryotaro Kamimura
IT Education Center and School of Science and Technology, Tokai Univerisity
4-1-1 Kitakaname Hiratsuka Kanagawa, 259-1292, Japan

***Abstract*—In this paper, we introduce a new type of information-theoretic method called "information-theoretic active SOM", based on the self-organizing maps (SOM) for training multi-layered neural networks. The SOM is one of the most important techniques in unsupervised learning. However, SOM knowledge is sometimes ambiguous and cannot be easily interpreted. Thus, we introduce the information-theoretic method to produce clearer and interpretable representations. The present method extends this information-theoretic approach into supervised learning. The main contribution can be summarized by three points. First, it is shown that clear representations by the information-theoretic method can be effective in training supervised learning. Second, the method is sufficiently simple where there are two separated components, namely, information maximization and error minimization component. Usually, two components are mixed in one framework, and it is difficult to compromise between them. In addition, the knowledge obtained by this information-theoretic SOM can be used to solve the shortage of unlabeled data, because the information maximization component is unsupervised and can process all input data with and without labels. The method was applied to the well-known image segmentation datasets. Experimental results showed that clear weights were produced and generalization performance was improved by using the information-theoretic SOM. In addition, the final results were stable, almost independent of the parameter values.**

***Keywords*—SOM; Labeled and Unlabeled; Supervised and Unsupervised; Generalization; Interpretation**

I. Introduction

The present paper aims to introduce a new type of information-theoretic method called "information-theoretic active self-organizing maps (SOM)" to improve generalization performance. The novelty and contribution of the new method can be summarized by three points, namely, the utility of information-theoretic SOM for supervised learning, simple and separated computation, and application to the target shortage problem.

A. Explicit Knowledge for Supervised Learning

First, the present paper aims to show the utility of using the information-theoretic SOM for supervised learning. Self-organizing maps (SOM) have been established as one of the most important unsupervised methods in neural networks [1], [2]. Knowledge obtained by the SOM and represented over connection weights has been exclusively used for the visualization of input patterns [3], [4], [5], [6], [7], [8]. However, one of the main problems is that SOM knowledge is sometimes ambiguous and hard to interpret [9], [10], [11], [12], [13], [14], [15], [16], [17], [18], [19]. Thus, contrary to its good reputation for visualization, practically it has been difficul to use and visualize SOM knowledge.

The information-theoretic SOM has been introduced to improve and clarify SOM knowledge [20], [21]. In this method, information on input patterns is increased while maintaining neighborhood relations between neurons. By controlling the information content of input patterns, connection weights can be modifie for better visualization. When this information content is increased, a smaller number of hidden neurons tend to represent input patterns. Because many input patterns are compressed into a smaller number of hidden neurons, it becomes easier to interpret the fina activities of hidden neurons. It has been observed that increased information content can improve the interpretation of neurons' behaviors.

The present paper tries to show that this knowledge by the information-theoretic method can be used to train neural networks in supervised ways. While the SOM was originally developed for unsupervised learning, the rich knowledge obtained by this method has stimulated a number of attempts to use it for supervised learning as well [22], [23], [24],[25]. However, they were not necessarily successful and it can be said that they could not reach the performance level of the conventional supervised learning methods. This is because SOM knowledge is itself created in unsupervised ways and not necessarily suited for training supervised neural networks. For this, the information-theoretic SOM has good potentiality, because the knowledge obtained by the method is much clearer than that by the conventional methods. The present paper tries to show the effectiveness of this clear representation for training supervised neural networks.

B. Simple and Separated Computing

The present method is well suited for the supervised SOM [24] [25] with simple and separated computing components. As above mentioned, the SOM knowledge has been used for supervised learning. However, these attempts have not necessarily been successful, because it is difficul to compromise between error minimization and competition processes. Though information-theoretic methods have been applied to supervised learning, one of the major problems is that information maximization is sometimes contradictory to error minimization between targets and outputs. Thus, it becomes difficul to compromise between those two contradictory procedures, especially when the problems become more complex. The present method solves this problem by separating the information maximization and error minimization components.

Borrowing procedures from the fiel of deep learning [26], [27], the present method separates the information maximization or unsupervised phase from the supervised information use phase. By virtue of this separation, each phase, unsupervised or supervised, can focus on its own main task of information maximization or error minimization.

C. Application to Label-Shortage Problem

Then, the present method can be applied to the so-called "label-shortage problem" [28], [29]. As is frequently pointed out, there is little labeled data, while unlabeled data are abundant. A variety of methods have been developed to handle the shortage of labeled data. Among them, the most important methods are semi-supervised learning and active learning. Both methods try to utilize the knowledge of unlabeled data to ameliorate the shortage of labeled data. Active learning tries to recruit the most informative unlabeled patterns to reinforce supervised learning [29]. On the other hand, in semi-supervised learning, information on unlabeled data is used to estimate the targets in explicit or implicit ways [28].

To cope with the "labeled data shortage" problem, we can use the knowledge generated by the information-theoretic SOM, since it can be produced in unsupervised ways. As mentioned above, the two phases of learning, namely, the information maximization and error minimization phases, are separated. In the firs information maximization phase, the information-theoretic SOM is applied to obtained knowledge on input patterns with and without labels. Then, in the supervised phase, this knowledge is used to train connection weights for supervised learning. Similar methods have been proposed for semi-supervised learning, for example, the use of generative models to gain features for classificatio [30], [31]. The present method can use the rich knowledge through the information-theoretic SOM, which can be expected to produce much information on the entire input patterns.

D. Paper Organization

In Section 2, we present how to compute connection weights in both unsupervised and supervised ways. In the unsupervised phase, collective outputs from multiple hidden or competitive neurons are computed. Information maximization processes are realized in terms of decreasing Kullback-Leibler divergence between collected an individual outputs. In the supervised phase, the softmax learning procedures are used to produce update rules. In Section 3, the experimental results of the image segmentation data sets are shown from the well-known machine learning database. First, the most explicit connection weights are obtained by changing the number of winners. Then, generalization errors and the number of epochs are examined. Experimental results for the dataset show that improved generalization could be obtained with clearer connection weights. Compared with generalization by the conventional BP and support vector machines (SVM), the present method gave the better performance. In addition, these results were more stable than those by the conventional method.

II. Theory and Computational Methods

A. Information-Theoretic Supervised SOM

Figure 1 shows how the information-theoretic SOM is applied. In Figure 1(a), there is a small number of labeled data, while unlabeled data are abundant. In the unsupervised phase in Figure 1(b), all data (both labeled and unlabeled) are used for training the information-theoretic SOM. Then, in Figure 1(c), the connection weights by the unsupervised phase are transferred to the supervised learning phase. Taking those connection weights as initial weights, supervised learning is performed. Naturally, the supervised learning is conducted only with labeled data. The problem is whether SOM knowledge by all data (labeled and unlabeled) can be effective in improving performance.

B. Basic Components

As shown in Figure 1, a network is composed of an input layer, competitive layer and output layer. Let us explain how to compute the output from the competitive and output neurons. Now, the sth input pattern can be represented by $\mathbf{x}^s = [x_1^s, x_2^s, \cdots, x_L^s]^T,\ s = 1, 2, \cdots, S$. Connection weights into the jth competitive neuron are denoted by $\mathbf{w}_j = [w_{1j}, w_{2j}, \cdots, w_{Lj}]^T,\ j = 1, 2, \ldots, M$. The output from an output neuron is computed by

$$v_j^s = \exp\left(-\frac{\| \mathbf{x}^s - \mathbf{w}_j \|^2}{2\sigma^2}\right), \tag{1}$$

where σ denotes the spread parameter.

In the output layer, we use the sofmax output computed by

$$o_i^s = f\left(\sum_{j=1}^{M} W_{ji} v_j^s\right) \tag{2}$$

where W_{ji} are connection weights from the competitive neurons of the last competitive layer to the output ones.

C. Unsupervised Phase

In the unsupervised phase, the individual neurons try to imitate the outputs by multiple winners to realize self-organization. By normalizing the output, we have the firin probability

$$p(j \mid s) = \frac{v_j^s}{\sum_{m=1}^{M} v_m^s}. \tag{3}$$

In addition to this firin probability, the output by multiple neurons or winners is used to realize cooperation between neurons as done in the SOM. Now, suppose that the neurons c_1, c_2 are the firs and the second winners, and so on. Then, the corresponding outputs can be ranked as follows:

$$v_{c_1} > v_{c_2} > \ldots > v_{c_M}. \tag{4}$$

Following the formulation of SOM, the distance between the winner and the other neurons is computed by

$$\phi_{jc_1} = \exp\left(-\frac{\| \mathbf{r}_j - \mathbf{r}_{c_1} \|^2}{2\sigma_{ngh}^2}\right), \tag{5}$$

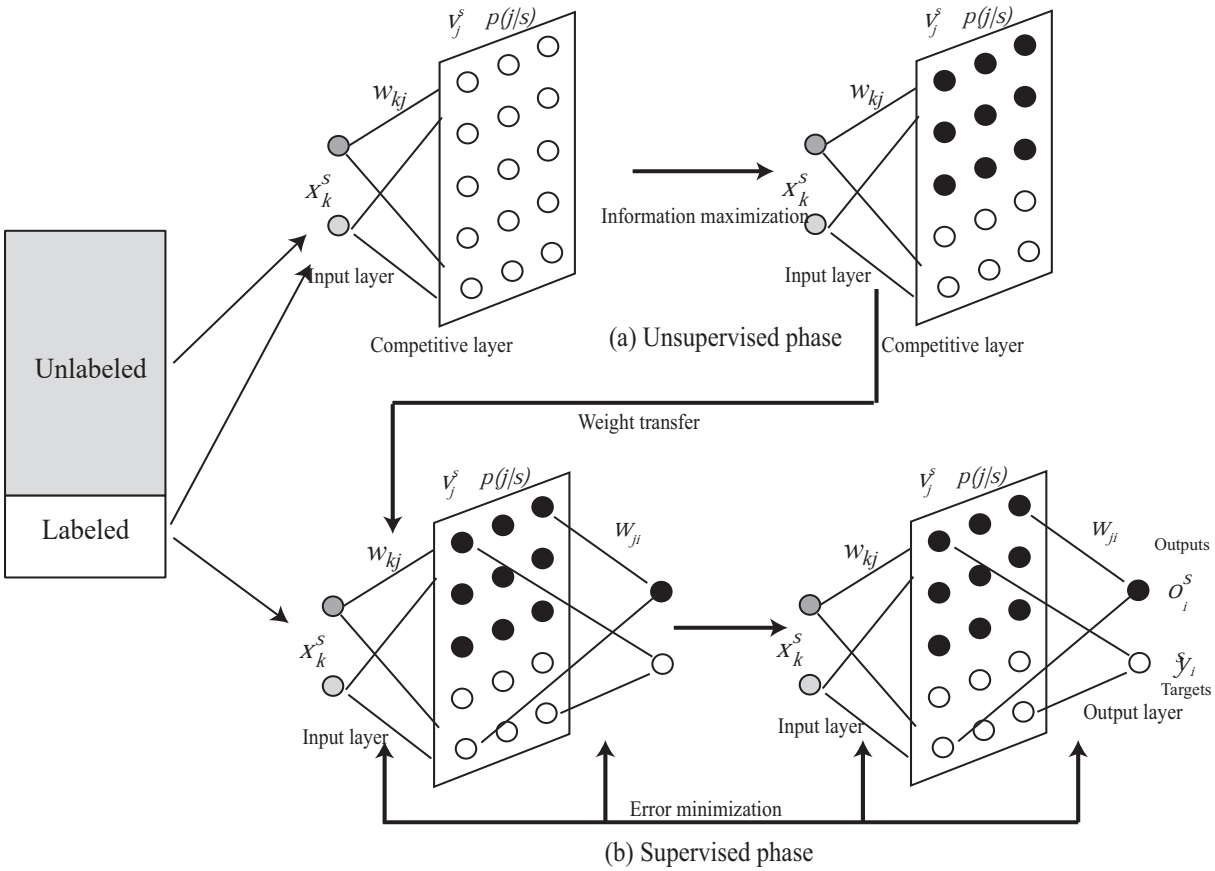

Fig. 1. Learning processes for the information-theoretic supervised SOM with the unsupervised (a) and supervised (b) phase.

where $\mathbf{r}_j$ denotes the position of the jth neuron on the output map and σ_{ngh} is the spread parameter. The jth neuron's output is the weighted sum of R winners' outputs and computed by

$$z_j^s(R) = \sum_{m=1}^{R} \phi_{jc_m} v_{c_m}. \tag{6}$$

The firin probability by the multiple winners is define by

$$q(j \mid s; R) = \frac{z_j^s(R)}{\sum_{j=1}^{M} z_m^s(R)}. \tag{7}$$

Learning should be performed to reduce the difference between these outputs. This difference using the Kullback-Leibler divergence is computed by

$$KL = \sum_{s=1}^{S} p(s) \sum_{j=1}^{M} p(j \mid s) \log \frac{p(j \mid s)}{q(j \mid s; R)}. \tag{8}$$

In addition to the KL divergence, there are the other errors which must be minimized, namely quantization errors between connection weights and input patterns

$$Q = \sum_{s=1}^{S} p(s) \sum_{j=1}^{M} p(j \mid s) \|\mathbf{x}^s - \mathbf{w}_j\|^2. \tag{9}$$

Fixing this quantization error and minimizing the KL-divergence, the optimal firin rates are computed by

$$p^*(j \mid s) = \frac{q(j \mid s; R) \exp\left(-\frac{\|\mathbf{x}^s - \mathbf{w}_j\|^2}{2\sigma^2}\right)}{\sum_{m=1}^{M} q(m \mid s; R) \exp\left(-\frac{\|\mathbf{x}^s - \mathbf{w}_m\|^2}{2\sigma^2}\right)}. \tag{10}$$

In addition, for connection weights, the re-estimation formula [20] are obtained by

$$\mathbf{w}_j = \frac{\sum_{s=1}^{S} p^*(j \mid s) \mathbf{x}^s}{\sum_{s=1}^{S} p^*(j \mid s)}. \tag{11}$$

D. Supervised Fine Tuning

In the output layer, the sofmax output is computed by

$$o_i^s = \frac{\exp\left(\sum_{j=1}^{M} W_{ji} v_j^s\right)}{\sum_{m=1}^{N} \exp\left(\sum_{j=1}^{M} W_{jm} v_j^s\right)}, \tag{12}$$

where W_{ji} are connection weights from the competitive neurons of the last competitive layer to the output ones. The error is computed by

$$E = -\sum_{s=1}^{S} \sum_{i=1}^{N} y_i^s \log o_i^s, \tag{13}$$

where y is the target and N is the number of output neurons. The error function is differentiated with respect to connection

weights in the competitive and output layer. The update formula for the firs competitive layer is shown by

$$\Delta w_{kj} = \frac{\eta}{S}\sum_{s=1}^{S}\delta_j^s(x_k^s - w_{kj}), \quad (14)$$

where δ is the error signal sent from the upper layers and η is a learning parameter.

III. Results and Discussion

A. Image Segmentation Data

1) Experiment Outline: The dataset of the image segmentation was taken from the well-known machine learning database [32]. The dataset was drawn randomly from a database of 7 outdoor images. The images were hand-segmented to create a classificatio for every pixel. The number of input patterns was 2310. The number of input neurons was 19 and the number of output neurons was seven, corresponding to the seven outdoor images. The number of competitive neurons was 5 by 12 neurons, as shown in Figure 2. The number of training patterns was increased from 10 to 100 to demonstrate the effect of the unsupervised information-theoretic method. The number of patterns for the validation set was 500, and the remaining patterns were used for testing (1710 patterns).

2) Improved Interpretation: First, we showed that the proposed method could produce more interpretable connection weights. Figure 3 shows U-matrices (1) and the corresponding labels (2) by the conventional method (a) and the information-theoretic method (b). By the conventional method in Figure 3(a), a clear class boundary in warmer colors could be seen on the upper side of the matrix. Another boundary, though weaker, was seen on the lower side of the matrix. However, by using the information-theoretic method with three winners in Figure 3(b), those class boundaries became stronger in warmer colors.

The same tendency was obtained for the connection weights, meaning that stronger characteristics could be seen by the information-theoretic method. Comparing connection weights by the SOM, some, in particular those in Figure 4(b6), (b-9)-(b-12) were accentuated by the information-theoretic method .

3) Improved Generalization : We compared generalization performance of three methods, namely, the conventional BP, SVM and the information-theoretic method. For fair comparison, the SVM was fine-tuned the box constraint and kernel scale parameters were extensively changed to have the best possible results. As seen in Table I, the generalization errors by the information-theoretic method, including the average, minimum and maximum ones, were much lower than those by the conventional methods. For example, when the number of training patterns was the smallest (10 patterns), the average, minimum and maximum values were 0.620, 0.473 and 0.753 by the conventional method, and 0.732, 0.474 and 0.909 by the SVM, respectively. Those values decreased to 0.438, 0.280 and 0.620 by the information-theoretic method. The differences between them decreased when the number of input patterns increased. However, even if the number of input patterns increased to 100 patterns, the average, minimum and maximum values decreased from 0.185, 0.161 and 0.222 by the conventional method to 0.123, 0.110 and 0.144 by the information-theoretic method. Interestingly, the SVM gave the worst errors when the number of input patterns was 100. In addition, the standard deviation of the generalization errors was smaller by the information-theoretic method. The number of learning epochs was similar across both methods.

TABLE I. Summary of experimental results by the conventional BP, SVM and the information-theoretic method for the segmentation data set. The notation CNV and INF represent the conventional and information-theoretic methods, respectively.

Methods	Patterns	Generalization error				Epochs
		Average	Std dev	Min	Max	
CNV	10	0.620	0.098	0.473	0.753	468
	20	0.543	0.093	0.372	0.695	470
	30	0.433	0.100	0.264	0.581	445
	40	0.352	0.078	0.261	0.486	492
	50	0.291	0.080	0.187	0.451	480
	100	0.185	0.019	0.161	0.222	466
INF	10	0.438	0.098	0.280	0.620	316
	20	0.310	0.069	0.209	0.430	444
	30	0.249	0.062	0.168	0.337	396
	40	0.209	0.059	0.133	0.282	390
	50	0.181	0.041	0.131	0.260	466
	100	0.123	0.011	0.110	0.144	460
SVM	10	0.732	0.165	0.474	0.909	
	20	0.499	0.156	0.311	0.805	
	30	0.426	0.172	0.247	0.836	
	40	0.314	0.057	0.212	0.392	
	50	0.276	0.042	0.213	0.336	
	100	0.201	0.021	0.161	0.236	

4) Improved Stability: Our analysis showed that the fina values by the information-theoretic method were relatively stable, meaning that the generalization errors and the number of epochs were not relatively affected by the change in the parameter values.

Figure 5 shows the generalization errors by the conventional method in blue and by the information-theoretic method in red as a function of the parameter σ when the number of input patterns increased from 10 (a) to 100 (d). The generalization errors by the information-theoretic method in red were well lower than those by the conventional method in blue, particularly when the number of input patterns was smaller. Even if the number of input pattern was larger, the generalization errors by the information-theoretic method were lower than those by the conventional method, in particular when the parameter σ became smaller.

One of the most important things to note is that the generalization errors generated by the information-theoretic method were more stable than those by the conventional method. When the number of input patterns was ten, the generalization errors were higher for smaller values of the parameter σ. However, the generalization errors were almost constant for all values of the parameter σ. This tendency of stability became more apparent when the number of input patterns increased.

Figure 6 shows that the number of epochs produced the lowest validation errors when the number of training patterns increased from 10(a) to 100(d). By the conventional method, the number of epochs gradually increased when the parameter σ increased. On the other hand, the number of epochs by the information-theoretic method remained stable, almost independent of the parameter σ.

Finally, our method was able to effectively reduce the

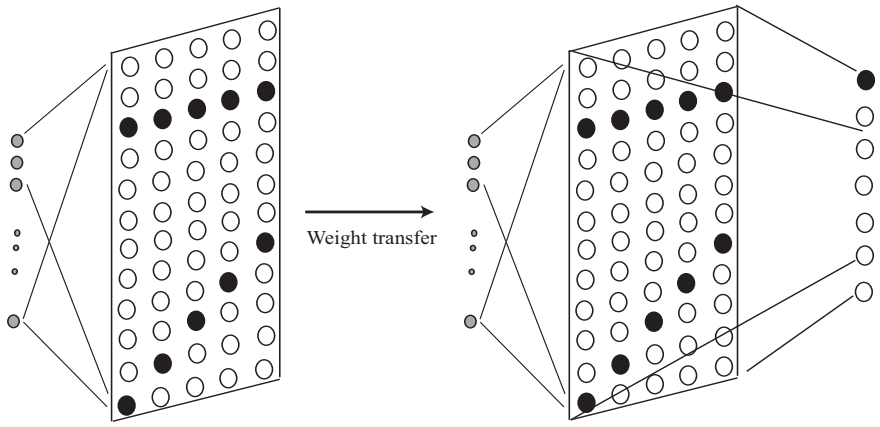

Fig. 2. Network architecture with 19 input neurons, 5 by 12 competitive and 7 output neurons for the image segmentation data.

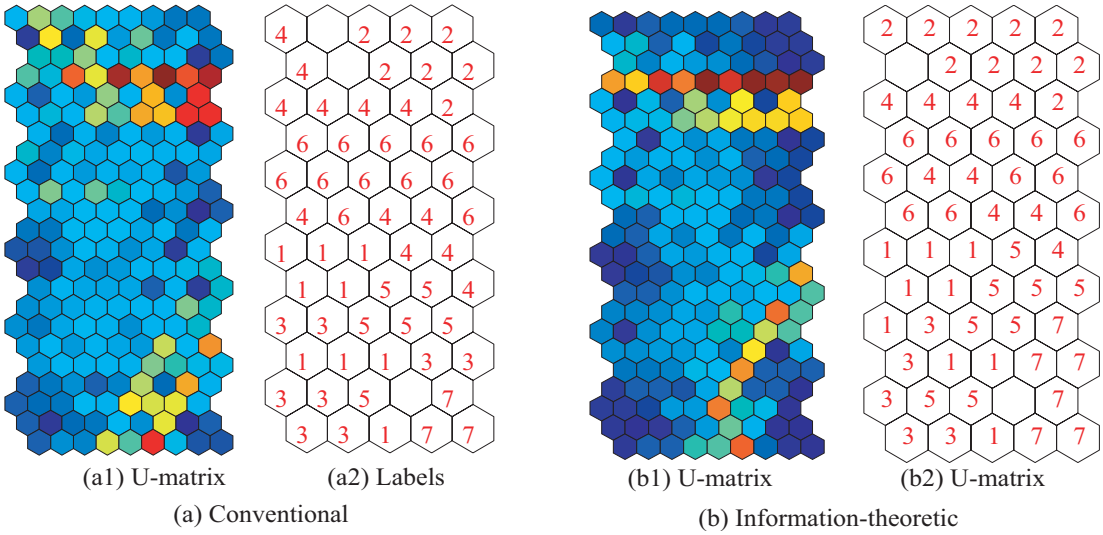

Fig. 3. U-matrices and labels by the conventional SOM (a) and when the number of winners was three (b).

number of errors in cases where the conventional method failed to do so. Figure 7 shows an example of learning processes. Without knowledge in Figure 7(a), learning was impossible. On the other hand, all errors became immediately smaller by the information-theoretic method.

B. Discussion

1) Validity of the Method and Experimental Results: In this paper, we showed that information obtained by the information-theoretic SOM can be used to improve generalization performance with a relatively smaller number of labeled input patterns. In the fiel of active and semi-supervised learning [30], [31], [33], there have been many attempts to use information content in unlabeled data for training neural networks. The present method suggests that the information-theoretic SOM can be used to train neural networks with information in unlabeled data.

The main results can be summarized by the following three points, namely, improved interpretability, generalization and stability. First, fina representations were easier to interpret when using the information-theoretic method. By appropriately increasing the number of winners, fina connection weights were well visualized by using the well-known U-matrix in Figure 3, though the number of winners had to be heuristically determined. The fina visualized weights showed much clearer maps than those by the conventional method.

Second, the clearer weights could be used to train multi-layered neural networks with better generalization performance. In particular, when the number of training patterns was smaller, improved generalization performance could be more explicitly observed. Figure 7 shows that learning was accelerated even when the learning itself was impossible by the conventional SOM. This suggests that knowledge obtained by the information-theoretic method can be used to train multi-layered neural networks.

Third, the fina results were obtainable almost independently of the parameter values. As shown in the experimental results in Figure 5, generalization errors were almost unchanged when the parameter σ was increased. On the other hand, by using the conventional multi-layered neural networks, drastic changes were observed when the parameter σ was changed. The present method, thus, could be used to stabilize learning processes via easy tuning of the parameters. In addition, in Figure 6, the number of training epochs to reach the lowest validation error showed the stable number of epochs by the present method. On the other hand, the conventional

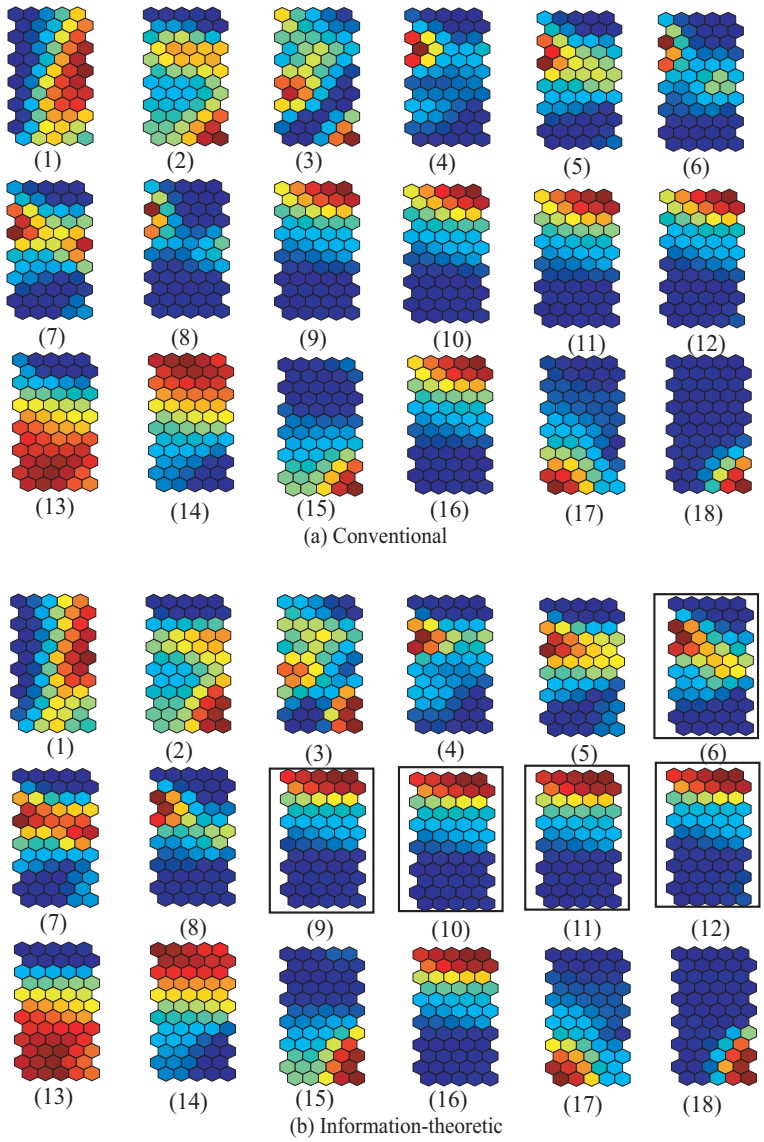

Fig. 4. Connection weights by the conventional SOM(a) and the information-theoretic method (b).

method showed drastic changes in the number of epochs.

The experimental results showed that the present method could utilize unlabeled data to train supervised networks. In addition, the results obtained by the present method were accompanied by explicit internal representations, permitting possible interpretation. The reason for this improved performance is due to the fact that self-organizing maps, based on competitive learning, aim to separate input patterns into several classes with an equal number of input patterns. Thus, the information-theoretic method classifie input patterns into several classes, and in the fina supervised phase, only minor adjustments need to be made to the connection weights for input patterns.

C. Problems of the Method

Though the present method demonstrated relatively greater stability and generalization, it has two problems, namely, the number of winners and relations between interpretability and generalization. Both are due to the absence of any explicit measure of interpretability.

First, the number of winners needed to determine the outputs is uncertain. As mentioned, the number of neurons is critically related to the clarity of fina internal representations. Thus, the number of neurons should be increased appropriately. However, because there are no explicit criteria to quantify the clarity of representations, the number of neurons was chosen very heuristically. Accordingly, some criteria for clear representations are needed for detecting the number of winners.

Second, relations between interpretability and generalization are also uncertain, because there are no criteria to ensure the clarity of representations. In the present paper, the clearest possible representations were intuitively chosen at the outset; then, the relations between them were examined. However, the intuitively clearest possible representations did not necessarily produce the best possible generalization performance. To examine the exact relations between interpretability and generalization, some criteria are needed to determine the clarity

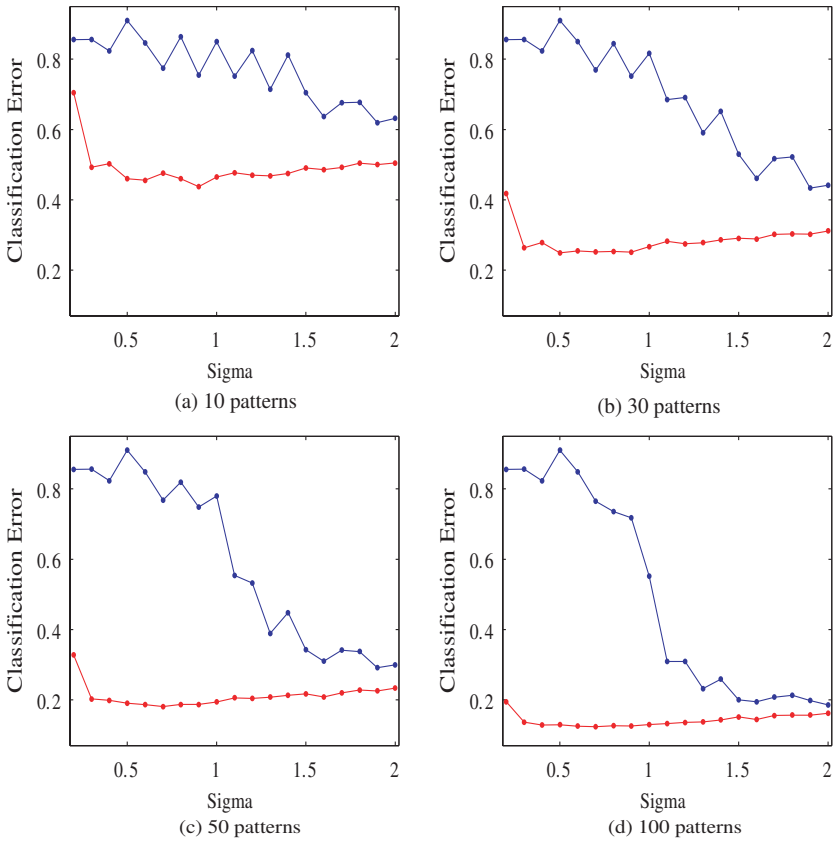

Fig. 5. The generalization errors by the conventional method in blue and by the information-theoretic method in red as a function of the parameter σ when the number of input patterns increased from 10 (a) to 100 (d).

of internal representations.

D. Possibility of the Method

The possibilities of the present method can be summarized by the following four points: interpretation, active learning, deep learning and self-organizing maps. First, the present method provides neural networks with improved interpretation performance. One of the main problems of neural networks is that it is impossible to interpret the fina representations obtained through learning [34], [35], [36], [37], [38], [39] [40], [41]. Even if novel new machine learning methods such as SVM, active and semi-supervised learning and deep learning show better performance in particular for generalization, it is practically impossible to interpret the fina results. The present method aims mainly to produce interpretable representations and to relate these representations to improved generalization. The method will be the firs step towards interpretation-oriented neural networks.

Second, in terms of active learning, the present method does not actively recruit input patterns to be labeled. It can thus be called "passive" learning. The next stage is to actively recruit the patterns to be labeled as done in active learning. In this case, the information content accumulated by the information-theoretic SOM can be used to choose candidate patterns to be labeled. This will be a new form of active learning which considers the information content stored in competitive neurons.

Third, in terms of deep learning, the present method is a form of shallow learning with only one hidden (competitive) layer. However, it is easy to extend this shallow model to a hierarchical deep model by adding multiple competitive layers. In this case, each layer added can be interpreted because the information-theoretic SOM has been developed to explicitly visualize connection weights. Thus, this is a new type of multi-layered network architecture for deep learning in which all hidden layers can be explicitly interpreted.

Finally, this paper suggests a new use for self-organizing maps. It has been shown that the information content by the information-theoretic SOM can be used to visualize only connection weights. However, in addition to visualization, the information obtained by the SOM can be used for many different purposes, such as training. Thus, the present method opens up a new possibility for using the SOM for different purposes.

IV. Conclusion

In this paper, it has been shown that the information-theoretic method can produce clear representations, and that the knowledge obtained by the information-theoretic SOM can be used to train supervised neural networks. Though the SOM

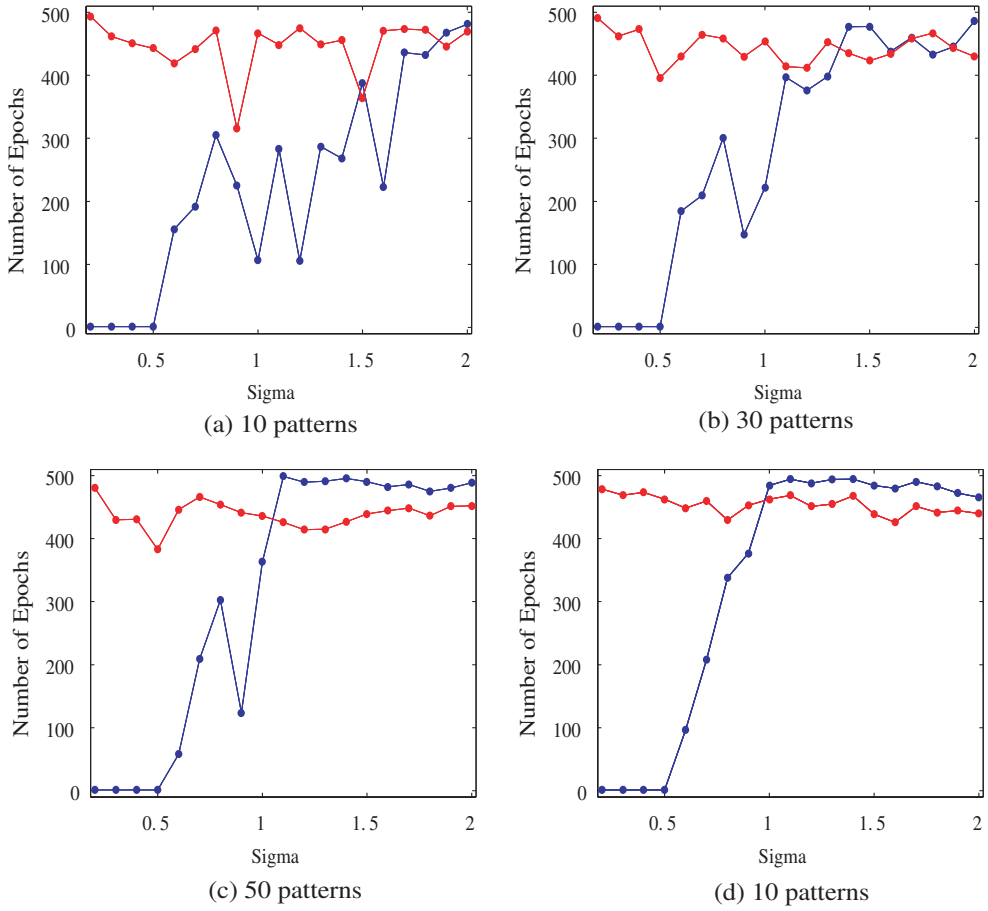

Fig. 6. The number of epochs by the method without knowledge in blue and with knowledge in red when the number of input patterns increased from 10 (a) to 100(d).

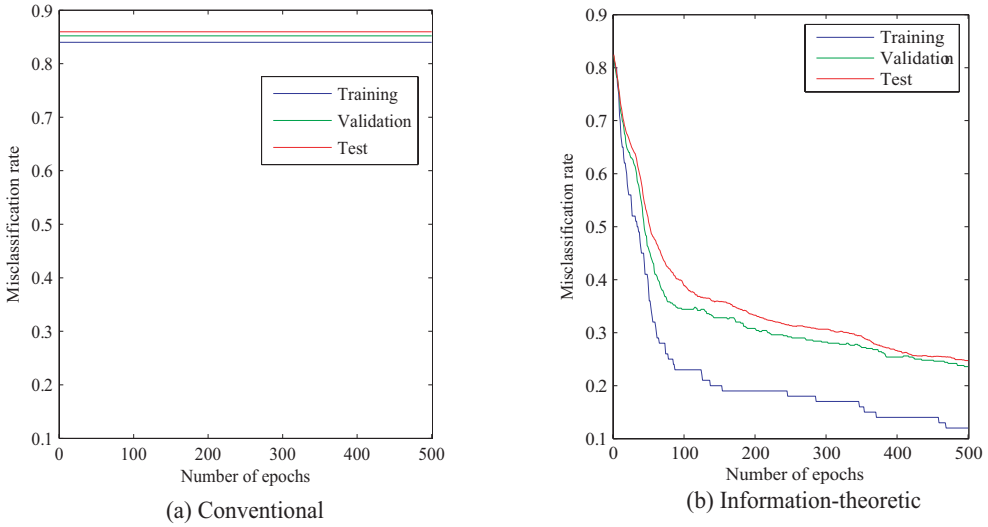

Fig. 7. Training (blue), validation (green) and testing (red) error rates by the method without knowledge by unsupervised learning (a) and with the knowledge (b), where the parameter σ was 0.2 and 100 patterns.

was developed to create more interpretable representations, it sometimes produces very ambiguous representations. The information-theoretic SOM was introduced in this paper to obtain more explicit and interpretable knowledge on input patterns. In addition, the method aimed to solve the shortage of labeled data problem. In actual situations, the amount of labeled date is scarce, and it is difficul to label unlabeled data. On the other hand, unlabeled data is abundant. Thus, the problem is to fin a method which can maximize the use of abundant unlabeled data. In the present method, the information-theoretic SOM acquires information content on input patterns in unsupervised ways, and can be used to over-

come the shortage of labeled data. Finally, the method aimed to solve the problem of compromising between error minimization of targets and outputs, and information maximization. It has been shown that error minimization is not necessarily used to increase information content in the information-theoretic sense. To solve this problem, the information acquisition and use phases are separated. Information was firs maximized in the acquisition phase, and then error was minimized in the information use phase. This separation showed better results for generalization and interpretation.

By applying the method to the image segmentation data sets from the machine learning database, favorable results were obtained and summarized by three points. The information-theoretic methods could produce much clearer internal representations which were accompanied by improved generalization. In particular, when the number of training patterns became smaller, the difference between our method and conventional ones become clearer. In addition, for all experimental results, the stabilization of learning processes was observed. This means that the number of learning epochs and generalization errors tended to be almost independent of the different values of the parameter. Applying the method to the image segmentation data sets revealed that it was able to produce more interpretable representations which were accompanied by improved generalization performance and stability.

However, one of the problems is that the relations between interpretability and generalization are uncertain. This means that though interpretability is roughly related to generalization performance, it is not necessarily accompanied by better generalization. To better relate interpretability to generalization, a method should be developed to unify the two concepts. In addition, the present method should be combined with some active learning techniques to recruit new input patterns to be labeled. Though the problems mentioned above should be solved, the present method nevertheless opened up new possibilities for using SOM knowledge.

REFERENCES

[1] T. Kohonen, *Self-organization and associative memory*, vol. 8. Springer Science & Business Media, 2012.

[2] T. Kohonen and P. Somervuo, "Self-organizing maps of symbol strings," *Neurocomputing*, vol. 21, no. 1, pp. 19–30, 1998.

[3] S. Kaski, J. Nikkila, M. Oja, J. Venna, P. Toronen, and E. Castren, "Trustworthiness and metrics in visualizing similarity of gene expression," *BMC Bioinformatics*, vol. 4, no. 48, 2003.

[4] J. Venna and S. Kaski, "Neighborhood preservation in nonlinear projection methods: an experimental study," in *Lecture Notes in Computer Science*, vol. 2130, pp. 485–491, 2001.

[5] G. Polzlbauer, "Survey and comparison of quality measures for self-organizing maps," in *Proceedings of the fifth workshop on Data Analysis (WDA04)*, pp. 67–82, 2004.

[6] J. A. Lee and M. Verleysen, "Quality assessment of nonlinear dimensionality reduction based on K-ary neighborhoods," in *JMLR: Workshop and conference proceedings*, vol. 4, pp. 21–35, 2008.

[7] T. Villmann, R. D. M. Herrmann, and T. Martinez, "Topology preservation in self-organizing feature maps: exact definitio and measurment," *IEEE Transactions on Neural Networks*, vol. 8, no. 2, pp. 256–266, 1997.

[8] H.-U. Bauer and K. Pawelzik, "Quantifying the neighborhood preservation of self-organizing maps," *IEEE Transactions on Neural Networks*, vol. 3, no. 4, pp. 570–578, 1992.

[9] J. Vesanto, "SOM-based data visualization methods," *Intelligent Data Analysis*, vol. 3, pp. 111–126, 1999.

[10] S. Kaski, J. Nikkila, and T. Kohonen, "Methods for interpreting a self-organized map in data analysis," in *Proceedings of European Symposium on Artificial Neural Networks*, (Bruges, Belgium), 1998.

[11] I. Mao and A. K. Jain, "Artificia neural networks for feature extraction and multivariate data projection," *IEEE Transactions on Neural Networks*, vol. 6, no. 2, pp. 296–317, 1995.

[12] C. De Runz, E. Desjardin, and M. Herbin, "Unsupervised visual data mining using self-organizing maps and a data-driven color mapping," in *Information Visualisation (IV), 2012 16th International Conference on*, pp. 241–245, IEEE, 2012.

[13] S.-L. Shieh and I.-E. Liao, "A new approach for data clustering and visualization using self-organizing maps," *Expert Systems with Applications*, vol. 39, no. 15, pp. 11924–11933, 2012.

[14] H. Yin, "ViSOM-a novel method for multivariate data projection and structure visualization," *IEEE Transactions on Neural Networks*, vol. 13, no. 1, pp. 237–243, 2002.

[15] M.-C. Su and H.-T. Chang, "A new model of self-organizing neural networks and its application in data projection," *IEEE Transactions on Neural Networks*, vol. 123, no. 1, pp. 153–158, 2001.

[16] S. Wu and T. W. Chow, "Prsom: a new visualization method by hybridizing multidimensional scaling and self-organizing map," *Neural Networks, IEEE Transactions on*, vol. 16, no. 6, pp. 1362–1380, 2005.

[17] L. Xu, Y. Xu, and T. W. Chow, "PolSOM-a new method for multidimentional data visualization," *Pattern Recognition*, vol. 43, pp. 1668–1675, 2010.

[18] Y. Xu, L. Xu, and T. W. Chow, "Pposom: A new variant of polsom by using probabilistic assignment for multidimensional data visualization," *Neurocomputing*, vol. 74, no. 11, pp. 2018–2027, 2011.

[19] L. Xu and T. Chow, "Multivariate data classificatio using PolSOM," in *Prognostics and System Health Management Conference (PHM-Shenzhen), 2011*, pp. 1–4, IEEE, 2011.

[20] R. Kamimura, "Self-enhancement learning: target-creating learning and its application to self-organizing maps," *Biological cybernetics*, pp. 1–34, 2011.

[21] R. Kamimura, "Constrained information maximization by free energy minimization," *International Journal of General Systems*, vol. 40, no. 7, pp. 701–725, 2011.

[22] T. Kohonen, *Self-Organization and Associative Memory*. New York: Springer-Verlag, 1988.

[23] T. Kohonen, *Self-Organizing Maps*. Springer-Verlag, 1995.

[24] S. Ohno, S. Kidera, and T. Kirimoto, "Efficien automatic target recognition method for aircraft SAR image using supervised som clustering," in *Synthetic Aperture Radar (APSAR), 2013 Asia-Pacific Conference on*, pp. 601–604, IEEE, 2013.

[25] J. I. Titapiccolo, M. Ferrario, S. Cerutti, C. Barbieri, F. Mari, E. Gatti, and M. Signorini, "A supervised SOM approach to stratify cardiovascular risk in dialysis patients," in *XIII Mediterranean Conference on Medical and Biological Engineering and Computing 2013*, pp. 1233–1236, Springer, 2014.

[26] G. E. Hinton and R. R. Salakhutdinov, "Reducing the dimensionality of data with neural networks," *Science*, vol. 313, no. 5786, pp. 504–507, 2006.

[27] G. Hinton, S. Osindero, and Y.-W. Teh, "A fast learning algorithm for deep belief nets," *Neural computation*, vol. 18, no. 7, pp. 1527–1554, 2006.

[28] X. Zhu, "Semi-supervised learning literature survey," Tech. Rep. 1530, Compuer sciences, University of Wisconsin-Madison, 2005.

[29] B. Settles, "Active learning literature survey," *University of Wisconsin, Madison*, vol. 52, pp. 55–66, 2010.

[30] T. Jaakkola, D. Haussler, *et al.*, "Exploiting generative models in discriminative classifiers" *Advances in neural information processing systems*, pp. 487–493, 1999.

[31] A. Holub, M. Welling, and P. Perona, "Exploiting unlabelled data for hybrid object classification" in *Proc. Neural Information Processing Systems, Workshop Inter-Class Transfer*, vol. 7, 2005.

[32] K. Bache and M. Lichman, "UCI machine learning repository," 2013.

[33] A. Oyefusi, "Oil and the probability of rebel participation among youths in the niger delta of nigeria," *Journal of Peace Research*, vol. 45, no. 4, pp. 539–555, 2008.

[34] L. I. Nord and S. P. Jacobsson, "A novel method for examination of the variable contribution to computational neural network models," *Chemometrics and Intelligent Laboratory Systems*, vol. 44, pp. 153–160, 1998.

[35] A. Micheli, A. Sperduti, and A. Starita, "Analysis of the internal representations developed by neural networks for structures applied to quantitative structure-activity relationship studies of benzodiazepines," *Journal of Chemical Information and Computer Sciences*, vol. 41, pp. 202–218, 2001.

[36] D. E. Rumelhart, G. E. Hinton, and R. Williams, "Learning internal representations by error progagation," in *Parallel Distributed Processing* (D. E. Rumelhart and G. E. H. et al., eds.), vol. 1, pp. 318–362, Cambridge: MIT Press, 1986.

[37] M. Ishikawa, "Structural learning with forgetting," *Neural Networks*, vol. 9, no. 3, pp. 509–521, 1996.

[38] M. Ishikawa, "Rule extraction by successive regularization," *Neural Networks*, vol. 13, pp. 1171–1183, 2000.

[39] J. A. Alexander and M. C. Mozer, "Template-based procedures for neural network interpretation," *Neural Networks*, vol. 12, pp. 479–498, 1999.

[40] G. G. Towell and J. W. Shavlik, "Extracting refine rules from knowledge-based neural networks," *Machine learning*, vol. 13, pp. 71–101, 1993.

[41] R. Feraud and F. Clerot, "A methodology to explain neural network classification" *Neural Networks*, vol. 15, pp. 237–246, 2002.